submitted to the **Journal of Space Weather and Space Climate**
for publication under the Creative Commons Attribution 4.0 International License (CC BY 4.0)
Confidential manuscript - © The author(s)

The Space Weather Awareness Training Network

SWATNet

T. Barata[1], D. Del Moro[2], R. Erdélyi[3,4,5], J. Fernandes[6,7], R. Gafeira[1,8], M. K. Georgoulis[9,18], K. Murawski[10], A. Nindos[11], O. Oliveira[12], S. Patsourakos[11], K. Petrovay[4], S. Poedts[13,10], R. Vainio[14], A. Afanasiev[14], M. B. Korsós[15,4,5], A. Boiko[16], L. Annie John[14,13], S. Biswal[3,11], S. Bourgeois[1,3], S. Chierichini[3,2], G. Francisco[1,2], A. André-Hoffmann[11,3], E. Husidic[13,14], S. Koya[11,10], M. Kumar[10,17], R. Mugatwala[2,3], G. A. L. Nogueira[3,4], A. Wagner[17], E. Kilpua[17]

[1] Instituto de Astrofísica e Ciências do Espaço, University of Coimbra,3000 Coimbra
e-mail: mtbarata@uc.pt
[2] Department of Physics, University of Rome Tor Vergata, Via della Ricerca Scientifica 1, 00133 Roma, Italy
[3] Solar Physics and Plasma Research Centre (SP2RC), School of Mathematical and Physical Sciences, University of Sheffield, Hicks Building, Hounsfield Road, Sheffield, S37RH, UK
[4] Department of Astronomy, Eötvös Loránd University, Pázmány Péter sétány 1/A, H-1117 Budapest, Hungary
[5] Gyula Bay Zoltán Solar Observatory (GSO), Hungarian Solar Physics Foundation (HSPF), Petőfi tér 3, H-5700 Gyula, Hungary
[6] CITEUC, Geophysical and Astronomical Observatory, 3040-004 Coimbra, Portugal
[7] Department of Mathematics, University of Coimbra, 3000 Coimbra, Portugal
[8] Geophysical and Astronomical Observatory of the University of Coimbra, University of Coimbra, 3040-004, Coimbra, Portugal
[9] Johns Hopkins University Applied Physics Laboratory North Laurel, United States
[10] Institute of Physics, University of Maria Curie-Skłodowska, ul. Radziszewskiego 10, 20-031 Lublin, Poland
[11] Section of Astrogeophysics, Department of Physics, University of Ioannina, 45110, Greece
[12] CFisUC, Department of Physics, University of Coimbra, 3004-516 Coimbra, Portugal
[13] Centre for Mathematical Plasma-Astrophysics, Department of Mathematics, KU Leuven, Celestijnenlaan 200B, 3001 Leuven, Belgium
[14] Department of Physics and Astronomy, University of Turku, 20014 Turku, Finland
[15] University of Sheffield, School of Electrical and Electronic Engineering, Amy Johnson Building, Portabello Street, Sheffield, S1 3JD, UK
[16] VaBo Consult Ltd., Bulgaria,
[17] University of Helsinki, Department of Physics, Helsinki, Finland
[18] Academy of Athens, Research Center for Astronomy and Applied Mathematics, 11527 Athens, Greece (on leave)

This provisional PDF is the accepted version. The article should be cited as: J. Space Weather Space Clim., doi: 10.1051/swsc/2026020

ABSTRACT

Motivation and Aims: The main objectives of this paper are twofold: (1) to present the Space Weather Awareness Training Network (SWATNet), an innovative Marie Skłodowska-Curie Training Network designed to provide high-quality doctoral training in space weather, and (2) to highlight the scientific advances achieved within the project.

Methods: By combining cutting-edge research with structured international and intersectoral training, SWATNet reached fundamental advances in understanding space weather phenomena and trained a new generation of scientists equipped to tackle modern challenges in both research and industry.

Results: SWATNet delivered advancements in modelling solar eruptions and solar corona, and improved studies of the propagation and transport of Solar Energetic Particles, often utilising interdisciplinary methods. These include machine and deep learning, image processing, and various numerical modelling approaches. The research produced 26 peer-reviewed journal articles, along with various presentations at international conferences. In addition, SWATNet successfully completed its ambitious training programme on practical observatory and industry training.

Key words. Space Weather – Solar Activity – Corona and Heliosphere – Modelling and Forecasting – Artificial Intelligence – Machine Learning and Deep Learning

1. General description

Space weather primarily refers to dynamic variations in solar magnetism and the heliosphere that result in disturbances in planetary space environments, including their magnetospheres and ionospheres (Pulkkinen, 2007; Temmer, 2021). Space weather can significantly impact modern technological systems, both in space and on the ground, resulting in substantial economic losses (Eastwood et al., 2017; Schrijver et al., 2015). include disruptions in satellite operations, power transmission networks, and the propagation of navigation and communication signals. Additionally, space weather poses health risks to humans operating in space, particularly during extravehicular activities.

1.1. Motivation

Understanding the drivers of space weather across multiple domains and temporal scales is key to modern space exploration. As an interdisciplinary field, space weather research requires a comprehensive understanding of the underlying fundamental physical processes, as well as approaches that incorporate artificial intelligence and machine learning techniques (e.g., Camporeale, 2019) to achieve accurate and actionable forecasts. Addressing the related scientific and technological challenges requires experts with diverse backgrounds who are equipped with both scientific knowledge and technological skills. In addition, the global value of the space economy and the number of space-related companies are rapidly increasing (e.g., World Economic Forum; Punnala et al., 2024), creating a growing need for a skilled future workforce.

The European Union-funded Horizon Marie Skłodowska-Curie Innovative Training Networks (ITNs), now referred to as Doctoral Networks under the Horizon Europe programme, provided an ideal framework for conducting space weather-related research and educating experts for the modern job market. These international training networks typically consist of 5–10 beneficiary institutions, recruit 10–15 Early Stage Researchers (ESRs), and collaborate with several academic, public, and industrial partners. Their primary aim is to train a new generation of scientists who are creative, entrepreneurial, and prepared to pursue careers in both academic and non-academic institutions while helping to tackle—and ultimately solve—modern societal challenges.

We describe here the Space Weather Awareness Training Network (SWATNet), a Marie-Curie ITN funded under the Horizon 2020 programme. SWATNet was implemented as a European Joint Doctorate (EJD) ITN, in which all doctoral candidates pursued joint or double degrees through collaborations between two academic institutions located in different countries. The project commenced on March 1, 2021, and concluded on August 30, 2025, following a six-month extension. The consortium comprised ten academic institutions across eight European countries (Finland, Greece, Hungary, Belgium, the United Kingdom, Italy, Poland, and Portugal), as well as several industry partners recognised in the field of space weather. The network trained 12 PhD students, combining high-level scientific research with interdisciplinary and intersectoral training.

1.2. Aims

In SWATNet, we created a cutting-edge research program that integrated interdisciplinary techniques to maximise the novelty of the results and provide diverse career opportunities for the network's ESRs. To achieve this and broaden the network's scientific vision, we designed it to include both academic and industrial partners. Examples of interdisciplinary competencies that were particularly sought by the network were Machine Learning and Deep Learning, which are rapidly proliferating in heliophysics and space weather forecasting applications. In addition, the SWATNet approach involved establishing common principles, organising activities throughout the network, and implementing a carefully schemed joint supervision system that includes academic and non-academic mentors and a structured management strategy. The importance of disseminating results was strongly emphasised, and ESRs received extensive training and numerous opportunities to actively engage in these activities.

Scientifically, SWATNet advanced our understanding of the fundamental physical mechanisms and phenomena that drive space weather and improved forecasting of space weather in Earth's environment. Key areas of the network's focus were on modelling and observational analysis of solar flares (Benz, 2017), eruptive phenomena, such as Coronal Mass Ejections (CMEs; Webb and Howard, 2012), and solar energetic particle (SEP) events (Reames, 2023). Regarding scientific education and training, the project offered a wide range of activities, including schools and workshops with hands-on activities and practical observatory training. As required by the EJD funding scheme, each ESR also completed a 6- to 12-month secondment at their academic partner institution abroad. Each ESR also completed 2-3 months of industrial training.

2. The science of SWATNet

The primary scientific aim of the network was to advance space weather and heliophysics research, with a focus on CMEs, SEP events, and coronal dynamics. New insights were achieved in predicting the occurrence of solar flares using a range of precursors and ML / AI techniques (Projects 1, 3 & 10), estimating CME magnetic fields and flux rope dynamics (Project 2 & 6), understanding solar atmospheric heating (Project 5), modelling energetic particle acceleration and propagation in the corona and heliosphere (Projects 7 & 8), forecasting CME impact and arrival using semi-empirical and ML / AI methods (Projects 9 & 11), and assessing the long-term evolution of solar features (Projects 4 & 12). Additionally, SWATNet aimed to optimise the scientific output of existing and forthcoming research infrastructures that are either led by Europe or receive substantial investment from European sources, such as the Daniel K. Inouye Solar Telescope, Solar Orbiter, Parker Solar Probe, Proba III, and the European Solar Telescope, and to contribute to defining new ESA missions and instrumentation.

The network utilised a range of advanced research techniques and datasets. Examples of existing codes employed across different projects include the EUHFORIA simulation (EUropean Heliospheric FOrecasting Information Asset; Pomoell and Poedts, 2018) for 3D magnetohydrodynamic (MHD) modelling of the inner heliosphere and CMEs, the COCONUT model (COolfluid COroNa UnsTructured; Perri et al., 2022, 2023; Kuźma et al., 2023) for global 3D representation of the solar corona, and the Monte Carlo–based PARADISE code (PArticle Radiation Asset Directed at Interplanetary Space Exploration; Wijsen, 2020) for capturing the transport of energetic particles. Primary data sources included the Solar Dynamics Observatory (SDO) and Solar Orbiter missions.

Importantly, SWATNet developed several novel and improved software and modelling tools, including tools for identifying and tracking solar flux ropes from simulation data (Project 6), advanced particle transport codes (Project 8), and new mathematical morphology algorithms for detecting solar features (Project 12). Various ML/AI techniques were rigorously assessed using multiple performance metrics and scores (Projects 10 and 11).

This section presents the methodologies, data sources, and key scientific findings of each project.

– **Project 1: Pre-eruption magnetic configuration and eruption forecasting**

Project 1 aimed to improve our understanding of the pre-flare configuration in solar active regions (ARs) by analysing the evolution of small-scale brightening activity in pre-flare and non-flaring configurations. With the continuous improvement in the spatial and temporal resolution of space-borne instruments, the study of small-scale short-lived events, referred to as transient brightenings, has recently attracted significant interest. These weak brightenings, likely associated with magnetic reconnection, could carry information about or even play a direct role in flare triggering (e.g. Moore et al., 2001; Chifor et al., 2007; Kusano et al., 2012; Bamba et al., 2013; Chen et al., 2016; Bamba et al., 2017; Kusano et al., 2020; Massa and Emslie, 2022; Dissauer et al., 2023, 2025). We investigate differences between ”flare-imminent” and ”not-flare-imminent” configurations in ARs by monitoring weak events and have developed a method to monitor brightening activity in the Solar Dynamics Observatory’s Atmospheric Imaging Assembly (AIA) extreme ultraviolet (EUV) channels. Small-scale transient activity is then linked to changes in EUV intensity between consecutive image frames.

Our method can identify transient brightenings trough two thresholding techniques: a 3-σ method based on pixel-level intensity variations, and a uniform threshold method that detects brightenings with intensities invariably exceeding 2000 DN $\cdot$ s^{-1} (example of detected brightenings in the top and middle rows in Figure 1, respectively for ARs 11226 and 11429 from our case study presented below). The former method can detect most brightenings above the background activity, while the latter is more sensitive to higher-intensity brightenings. Once brightenings are detected, their spatial distribution is compared with the position of the ARs’ magnetic polarity inversion line (PIL) obtained following the methodology described in Schrijver (2007). This is because PILs are prime locations for magnetic reconnection, and transient brightenings may be signatures of the release of excess magnetic energy (e.g., Shibata and Magara, 2011; Georgoulis et al., 2024).

The methodology was applied to 24-hour intervals of two case-study ARs: one highly dynamic (AR 11429 with a field of view of 500 × 500 pixels), which hosted multiple X-class flares and a quiescent one (AR 11226 with a 500 × 300 pixel field of view), which only gave a C-class flare during the chosen interval. This study revealed significant differences between the ”flare-imminent” and ”not-flare-imminent” ARs. First, regarding the number of brightenings detected, the not-flare-imminent AR exhibited almost no uniform threshold brightenings, and approximately half as many 3-σ-detected brightenings compared to the flare-imminent AR. Second, the cumulative evolution of the intensity and unsigned magnetic flux (UMF) associated with the detected brightenings are an order of magnitude larger for the flaring AR in the case of the intensity and UMF of the 3-σ brightenings, but up to two orders of magnitude larger in the case of the uniform threshold brightenings (see bottom row in Fig. 1). Third, we compared intensive (i.e., spatially averaged) and extensive (i.e., spatially integrated) measures of brightening intensity. A clearer distinction between flare-imminent and non-flare-imminent configurations emerged from extensive measurements of brightening intensity and UMF, corroborating the conclusion from previous studies (Bobra and Couvidat, 2015; Bobra and Ilonidis, 2016; Welsch et al., 2009) that extensive parameters yield better results for studying flare behaviour.

The initial results obtained from our case study show promise in distinguishing between the two AR populations. It is worth noting, however, that brightenings detected by a uniform threshold reveal more pronounced differences. The purpose of this project is not necessarily to propose a new flare precursor, but rather to attempt to identify a distinct behaviour related to flare-imminent configurations from the statistical properties of small-scale transient activity. A follow-up study, currently underway, aims to validate initial findings and, hopefully, provide clues for short-term flare forecasting by applying this method on a much larger AR sample.

– **Project 2: Assessment of the near-Sun CME magnetic field**
The primary objective of Project 2 is to assess the near-Sun CME axial magnetic field using magnetic helicity and then use this result to benefit inner heliospheric propagation models. Understanding the near-Sun magnetic field strength of CMEs is crucial, as it plays a key role in shaping the early evolution of CME dynamics and their potential impact on geospace (Vourlidas et al., 2019b; Kilpua et al., 2019). However, there are no routine observations of near-Sun magnetic fields of CMEs. Patsourakos et al. (2016) introduced a method for indirectly estimating this magnetic field based on the conservation of magnetic helicity. By estimating the helicity accumulation in ARs and the helicity difference before and after an eruption, which is assumed to be transported away by the associated CME, combined with forward CME modelling in the outer corona, one gains valuable insights into the early CME magnetic field evolution. These insights can be used to constrain input parameters in inner heliospheric CME propagation models.

Following the methodology of Patsourakos et al. (2016) but with a more refined approach to estimating the helicity budget of the CME, we conducted a case study of a CME observed on March 10, 2022, from NOAA AR 12962 Koya et al. (2024). This event featured both remote sensing and in situ observations at 0.43 AU by Solar Orbiter and at 0.99 AU by WIND, enabling robust

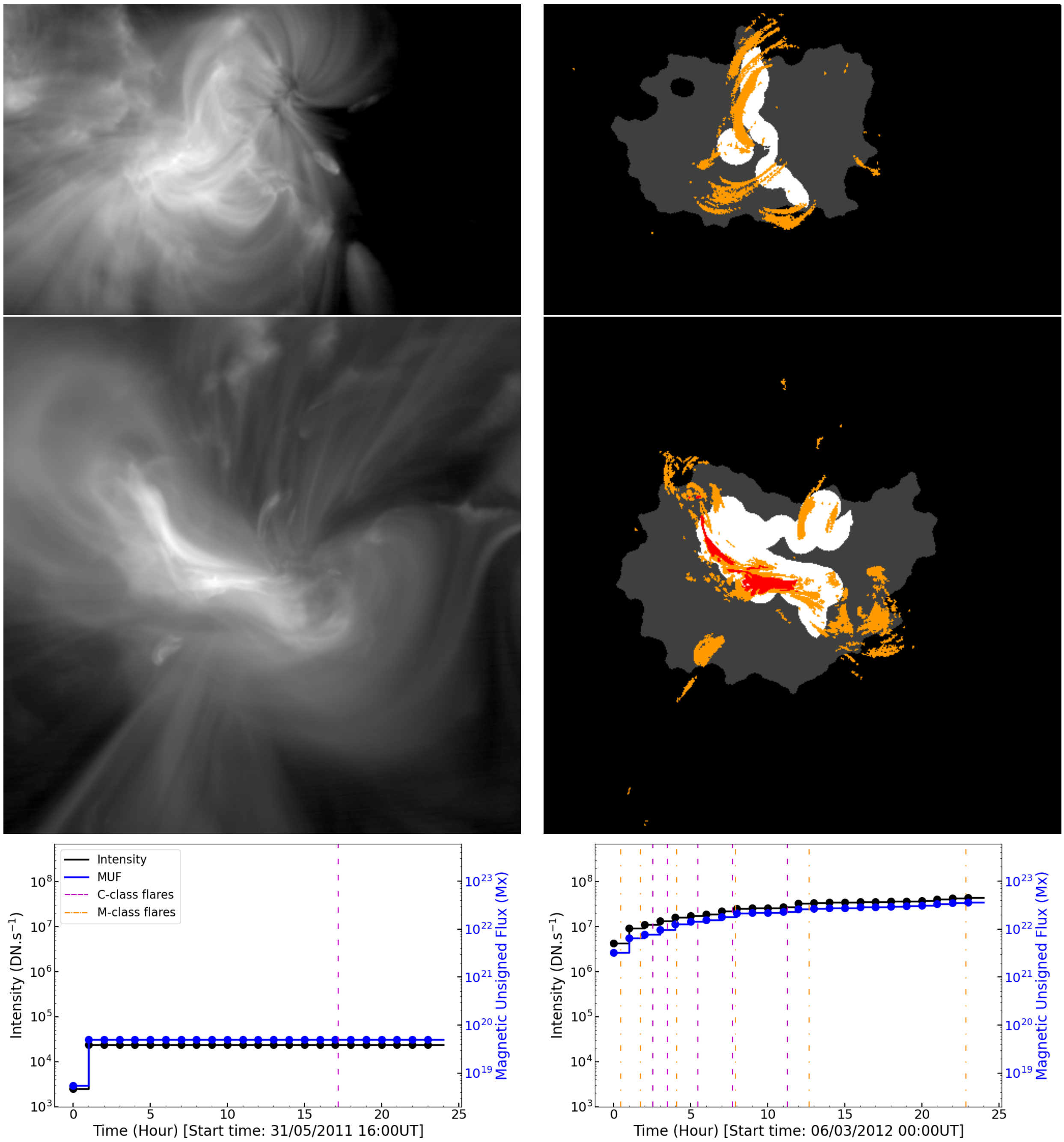

Fig. 1. *Top row*: 3-hour average 94 Å AIA image of AR 11226 (left) and the associated period masks (right) with the AR mask in grey, the PIL in white, the 3-σ brightenings in orange and the uniform-threshold brightenings in red. *Middle row*: 3-hour average 94 Å AIA image of AR 11429 (left) and the associated period masks (right). *Bottom row*: Cumulative evolution of the 94 Å AIA intensity (black) and magnetic unsigned flux (MUF; blue) associated with the uniform-threshold brightenings for ARs 11226 (left) panel and 11429 (right). Here, an hourly cadence was used.

cross-validation of magnetic field magnitude variations as a function of heliocentric distance at these two vantage points. From the temporal evolution of the instantaneous relative magnetic helicity of AR 12962, obtained using the connectivity matrix method of Georgoulis et al. (2012), we report a significant (i.e., above applicable uncertainties) difference in helicity between the pre- and post-eruptive phases of the AR. Using the Lundquist flux-rope model (Lundquist, 1950) and geometrical parameters derived from the Graduated Cylindrical Shell (GCS) (Thernisien et al., 2008; Thernisien et al., 2009) forward modelling, we determined the CME's axial magnetic field at the GCS-fitted height of 7.6 $R_{\odot}$ (0.03 AU) as 2067 $\pm$405 nT. Assuming a power-law dependence of the axial magnetic field with heliocentric distance (Bothmer and Schwenn, 1998; Wang et al., 2005; Farrugia et al., 2005; Demoulin and Dasso, 2009; Winslow et al., 2015; Patsourakos and Georgoulis, 2016), we extrapolated the near-Sun axial field to in situ measurements at 0.43 AU and 0.99 AU. We obtained a power-law index of -1.23 ± 0.18 for the magnetic-field variation between 0.03 AU and 1 AU, thereby improving upon existing studies that typically cover magnetic field magnitude variations in the 0.3-1 AU range. Our results indicate a less steep decline in magnetic-field strength with distance than reported in earlier studies (Leitner et al., 2007; Good et al., 2019; Salman et al., 2020); however, they agree with those incorporating near-Sun in-situ measurements, such as data from the Parker Solar Probe, as in Salman et al. (2024).

Based on our understanding of the helicity content of the 10 March 2022 CME (Koya, S. et al., 2026), we propose a new method to constrain the CME toroidal flux in the spheromak CME model (Verbeke et al., 2019) in the European Heliospheric Forecasting Information Asset (EUHFORIA) (Pomoell and Poedts, 2018) by using the magnetic helicity content of CMEs. By relating the magnetic helicity of the CME to its axial field in the spheromak model, we identify the axial field strength along the spheromak's axis ($B_{\text{spheromak}}$). The toroidal magnetic flux is derived from $B_{\text{spheromak}}$ and the CME's geometrical parameters. Our new method, which derived magnetic flux from the CME's helicity, effectively reproduces magnetic field strength in in situ measurements at 0.43 AU and 0.99 AU. When compared with in-situ measurements, the peak magnetic field magnitude at 0.99 AU is underestimated by ~19%, and by ~47% at 0.43 AU as seen from Fig.2. The power-law index with which the magnetic field magnitude is found to vary from the simulation insertion distance of 21.5$R_{\odot}$ to 2 AU is -1.63 ± 0.06.

Our study confirms a difference in helicity between the pre- and post-eruption states of the source AR, supporting the idea that helicity variations in ARs can serve as a quantitative diagnostic tool for CME eruptions. A well-constructed database containing the necessary information to infer near-Sun CME axial magnetic field values is essential for routine estimation of this diagnostic. Our methodology, when applied to such a database, can provide maximum-likelihood estimates of CME input parameters for inner-heliospheric propagation models.

– **Project 3: Three-dimensional solar flare forecasting**
Recent studies have shown that certain diagnostic parameters such as WG_M (a quantitative measure of the magnetic complexity of solar ARs - see Korsós et al., 2015), as well as magnetic helicity, could improve flare prediction time by 2-8 hrs if studied at certain height ranges of 1-1.8 Mm and 0.36-1.5 Mm above the photosphere (Korsós et al., 2020; Korsós et al., 2022). Motivated by these results, our main objective is to move one step beyond the traditional approach of studying the photospheric temporal variation of flare/CME precursors, and test their temporal variation at multiple heights in the lower solar atmosphere (up to ~ 3000 km). To do this, we performed a Potential Field (PF) extrapolation (Alissandrakis, 1981) of the radial component of the mag-

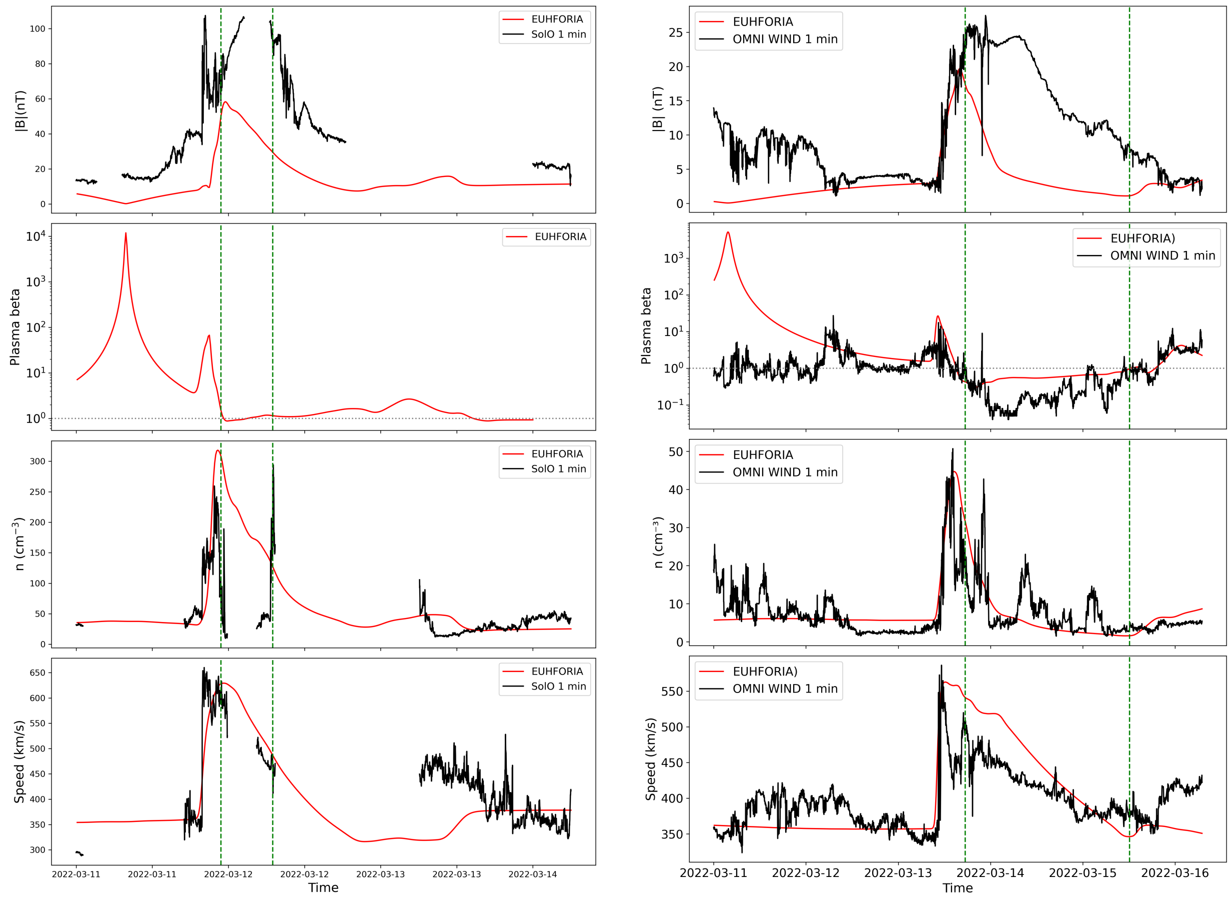

Fig. 2. Comparison of the model results with the in situ magnetic field strength and plasma properties such as the plasma beta, number density and speeds at 0.43 AU (left column). The black solid curves denote SolO measurements, while the red solid curves are model outputs. The vertical green dashed lines mark the time of the estimated magnetic cloud boundaries, within which the plasma β (equal to the ratio of gas to magnetic pressures) becomes less than 1 in the simulation. The right column contains the same information, but for the WIND data at 0.99 AU. This figure is adopted from Koya, S. et al. (2026).

netic field (B_r) up to 3.24 Mm (see Figure 3a) with a step size of 0.36 Mm (~ 0.5 arc-sec) and computed four different potential precursors closely related to PILs, namely, the (i) unsigned magnetic flux within 2 Mm of PILs (ϕ); (ii) R-value, namely an estimate of unsigned flux close to PILs associated with a high horizontal gradient in the vertical magnetic field (Schrijver, 2007); (iii) the total length of PILs (L_{tot}); and (iv) the maximum length of PILs (L_{max}). Sunspot complexity is correlated with flare productivity (see, e.g., Sammis et al., 2000) and thus we limited our analysis to only those sunspot complexes that hosted a δ-type magnetic configuration, indicating high morphological complexity. While the analysis was carried out for three different GOES (Geostationary Operational Environmental Satellite) flare classes (X/M/C), our main focus was on the strongest flaring category, i.e., X-class flares.

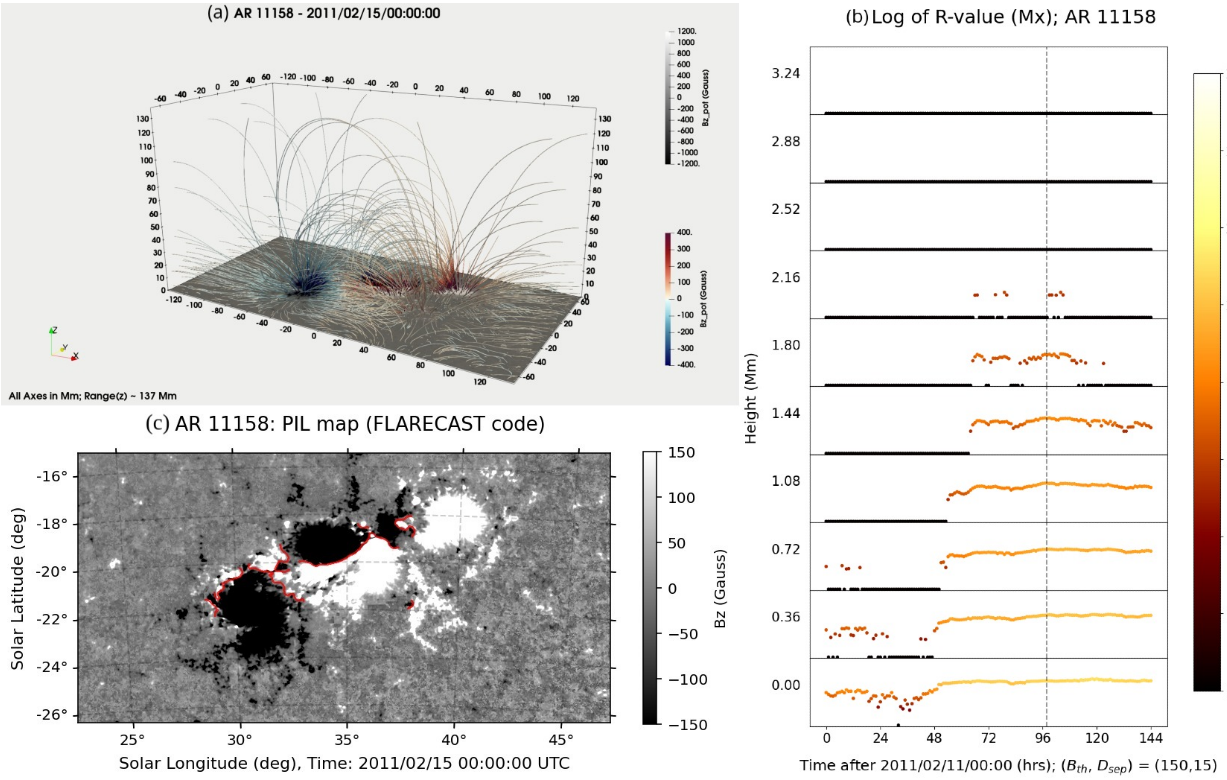

Fig. 3. (a) Visualisation of the photospheric B_r for AR 11158 extrapolated up to an altitude of 137 Mm at 00:00 UTC on 15 Feb, 2011. The colorbar on the top shows the strength of B_r, while the colorbar on the bottom shows the strength of the extrapolated magnetic field (B_z); (b) height-wise evolution of the R-value shows a clear jump from within a height range of 0.36 - 1.44 Mm for AR 11158. The colorbar shows the logarithm of the magnitude of the R-value (Mx). In this case, the jump in the R-value occurs approximately 49 hr before the first X2.2 flare on Feb 15, 2011; (c) identified PILs (in red) overlaid on the photospheric B_r as shown in (a), with field strength depicted in the colorbar. Plots (a) and (b) are adapted from Biswal et al. (2024).

From a study of 8 different ARs, our results show that the R-value may exhibit a significant jump approximately 48-68 hours prior to the first X-class flare for emerging ARs, i.e. ARs associated with increasing unsigned flux (Biswal et al., 2024). This behaviour, i.e. a sustained jump in the R-value, was detected across a range of heights (between 0.36-3.24 Mm in general, see example in Figure 3b). Further, the temporal variation of the R-value prior to X-class flares was significantly different for flaring vs. non-flaring cases (in terms of a jump in R-value), making it a promising tool for discriminating between flaring and non-flaring regions in the Sun (Biswal et al., 2024).

We also performed a height-wise analysis of PIL length parameters L_{tot} and L_{max} for a 48 hr time interval prior to the first flare (see Figure 3c for a PIL detection sample). Preliminary results show that the variation in these parameters can be modelled using simple, low-order autoregressive models in most cases. We also investigated the presence of stationarity in the time evolution of the PIL length parameters, i.e., whether the mean and variance of these parameters did not change significantly with time prior to eruption, to understand the morphological dynamics of

PILs. We found that in the majority of cases, the time series data was non-stationary.

– **Project 4: Modelling periodic and quasi-periodic variations in solar activity**
This project aimed to elucidate the complex interactions among nonlinear feedback effects and stochastic fluctuations, including rogue ARs and regions with atypical magnetic properties, to understand the long-term variation in solar cycle amplitudes and, consequently, space climate conditions.

Two candidate mechanisms have recently been considered for the nonlinear modulation of solar cycle amplitudes. Tilt quenching (TQ) is a negative feedback between the cycle amplitude and the mean tilt angle of bipolar active regions relative to the azimuthal direction; latitude quenching (LQ) consists of a positive correlation between the cycle amplitude and average emergence latitude of active regions. These effects are based on empirical correlations between cycle amplitude and the average latitude and tilt angle of ARs. In the case of LQ, in stronger cycles, ARs are, on average, positioned slightly further away from the equator, which allows for less leading polarity flux to reach the other hemisphere: hence, a larger fraction of the AR flux will cancel, and the contribution to the Sun's global dipole moment will be lower. In stronger cycles, ARs tend to have a lower tilt angle, resulting in a lower contribution to the Sun's dipole moment.

In one study (Talafha et al. 2022), we explored the relative importance of and the determining factors behind the LQ and TQ effects. The degree of nonlinearity induced by TQ, LQ and their combination was systematically probed in a grid of surface flux transport (SFT) models. The role of TQ and LQ was also explored in the successful 2x2D dynamo model. It was found that the relative importance of LQ vs TQ is governed by the dynamo effectivity range λ_R, which in turn is determined by the ratio of equatorial meridional flow divergence to magnetic diffusivity (Figure 4). The relative importance of LQ vs TQ scales as $c_1 + c_2/\lambda_R^2$, where c_1 and c_2 are constants.

As the buildup of the new poloidal field proceeds in the declining phase of a solar cycle, the prediction of the final dipole becomes ever more reliable, opening the possibility to extend the time horizon of the widely used precursor-based cycle forecasting backwards. We performed an extensive performance analysis of polar predictors, based on both observational data (WSO magnetograms, MWO polar faculae counts and Pulkovo A(t) index) and outputs (polar cap magnetic flux and global dipole moment) of various existing flux transport dynamo models. Setting a minimum value $r = 0.8$ for the correlation coefficient between predictor and predicted peak sunspot number as a lower limit for acceptable predictions, we find that observations and models alike indicate that the earliest time when the polar predictor can be safely used is 4 years after the polar field reversal. This is typically 2–3 years before solar minimum and about 7 years before the predicted maximum, considerably extending the temporal scope of the polar precursor method.

Besides nonlinear feedback mechanisms, stochastic fluctuations due to the randomness of AR emergence is another key factor behind the varying amplitude of solar cycles. A proper understanding of the statistical laws describing the distribution of individual ARs responsible for this stochasticity is a prerequisite for identifying major outliers or rogue ARs, as well as for realistically modelling the stochastic source term in space climate models. The systematic variation of solar AR properties with size, as measured by magnetic flux, has been the subject of numerous studies, yet the proposed scaling laws still vary widely. Constraining these laws and providing

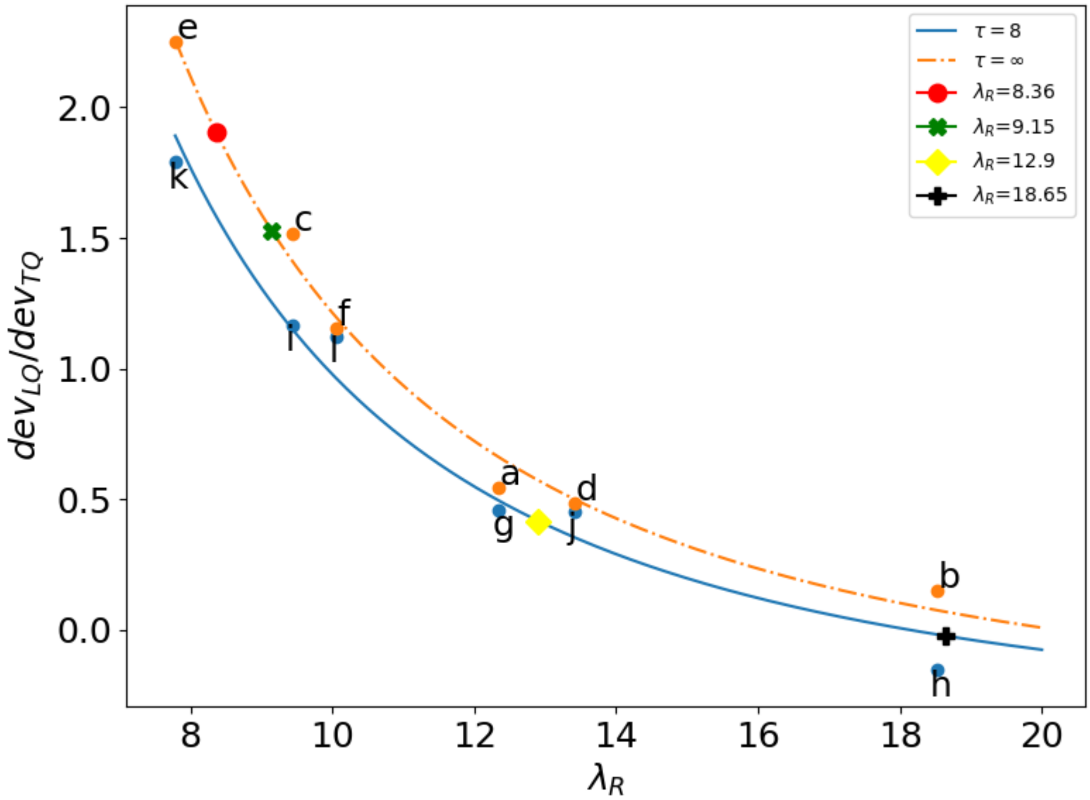

Fig. 4. Relative importance of latitude quenching vs. tilt quenching as a function of the dynamo effectivity range λ_R.

a statistical characterisation of the fluctuations about the mean laws are important for modelling the source term in surface flux transport and dynamo models of space climate variation, it may also help constrain the subsurface origin of active regions, as the scaling relations are expected to differ, depending whether AR structure is governed by the buoyant rise of a magnetic flux loop from the deep convective zone or by the action of magnetic and Coriolis forces on flux concentrations in near-surface layers. In a recent study (Nogueira et al. 2026), we determined AR scaling laws based on the recently constructed ARISE active region database listing bipolar ARs for cycles 23, 24 and 25. For the area A, polarity separation d and tilt angle γ, we found the following scaling against magnetic flux Φ and heliographic latitude λ: $A \sim \Phi^{0.84}$; $d = 3\overset{\circ}{.}35 \log(\Phi - \Phi_0)$; $\gamma \sim 28\overset{\circ}{.}62 \sin\lambda$ where $\Phi_0 = 2.22 \cdot 10^{20}$ Mx. These scaling relations are recommended for use in space climate research to model future data, fill in missing past data, and identify candidate rogue ARs.

– **Project 5: Global MHD coronal model**
The sharp rise in the plasma temperature in the solar atmosphere from about 5700 K at the base of the photosphere to 1 – 3 MK in the corona, and the origin of the solar wind, remain among the most long-standing problems in space physics. MHD waves are widely proposed as a potential mechanism for the observed heating in the two-fluid plasma, which is understood to be caused by convective motion beneath the surface of the Sun, that shakes the magnetic field lines extended

outward to the upper solar atmosphere. These waves, along with other processes such as jets and spicules, can transport energy, mass, and momentum throughout the solar atmosphere by converting kinetic and magnetic energy into thermal energy via dissipative mechanisms, including collisions between ions and neutrals. This project aimed to model the upper solar atmosphere layers by using the existing cutting-edge multi-fluid chromospheric models through the employment of the JOANNA code (Wójcik et al., 2019) for the local modelling and COolfluid COroNa UnsTructured MHD code (COCONUT; Perri et al., 2022, 2023) for global modelling of the solar atmosphere.

In the first part of the project, *the local aspect* was devoted, and we performed two-and-a-half-dimensional numerical simulations of two-fluid plasma in the solar chromosphere, concerning the dissipation of MHD waves that resulted from a localized pulse launched in the horizontal components of ion and neutral velocities from the top of the photosphere (Kumar et al., 2024a). In these simulations, the solar gravity pointed along the negative y-axis, the x-axis was horizontal, and the system remained invariant along the z-axis.

We explicitly detected fast and slow magneto-acoustic waves (MAWs) and Alfvén waves in a two-fluid system and explored two cases of transverse magnetic fields: (a) $B_z = 0$ Gs for MAWs and (b) $B_z = 2$ Gs for the linearly coupled Alfvén waves and MAWs. The obtained results showed that in the (b) case, the excited MHD waves were more effective at chromospheric heating than MAWS alone in the (a) case. In the developed model, we utilised ion-neutral collisions as the sole mechanism for wave energy dissipation; therefore, to better describe the solar atmosphere, more accurate simulations were required to account for additional non-ideal and non-adiabatic effects. We performed such simulations in the second part of the local aspect studies, which focused on numerical simulations of waves generated by incorporating more realistic solar conditions using a two-dimensional magnetic arcade (Kumar et al., 2024b). Unlike in the impulsive case, here the driver of the waves was the solar granulation itself, which was self-generated and self-evolved in the photosphere. The convective instabilities naturally excited a spectrum of waves. The results demonstrated that as these waves travelled through the chromosphere, collisional friction converted part of their energy into heat, raising the plasma temperature and increasing plasma outflows.

Our studies of local solar models consistently revealed that waves generated by either impulsive events or continuously operating solar granulation contribute to chromospheric heating. The released thermal energy compensated for energy losses, and the accompanying pressure gradients drove plasma outflows. The developed models provided insight into wave propagation, their dissipation, and the subsequent roles in plasma heating and accompanying plasma outflows. See Fig. 5 for sample results.

In the second part of the project, we finally developed *the global model* with implemented source and sink energy terms to account for the cumulative impact of transient events, such as indicated by the above-mentioned local simulations. The concept implied in the global model was that the energy input from numerous events, like ion-neutral drift, nanoflares, compressional, turbulent, and shock heating, all ultimately powered by the magnetic field of the Sun, can be treated as a continuous heat source. We extended this concept by including similar physics in the ion and neutral energy equations. To connect the explicit solvers included in the developed local models to the global model, we utilized empirical terms, specifically coronal heating, thermal

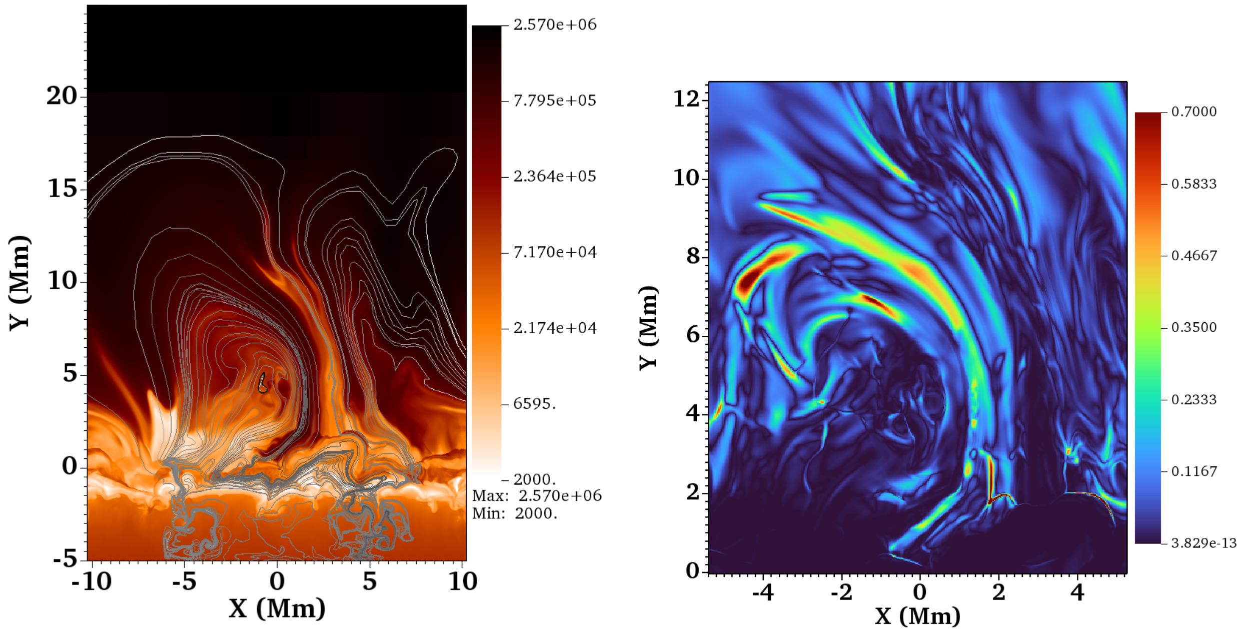

Fig. 5. The spatial distribution of the temperature of ions, log $T_{\rm i}$, expressed in MK, overlaid by magnetic lines (left) and a value of ion-neutral velocity drag, $|V_{\rm i} - V_{\rm n}|$, in km s^{-1} (right). The background state in *the local model*, initially specified by the hydrostatic equations with the arcade magnetic field, was altered by the self-generated and self-evolved solar granulation in the case of *the local model.*

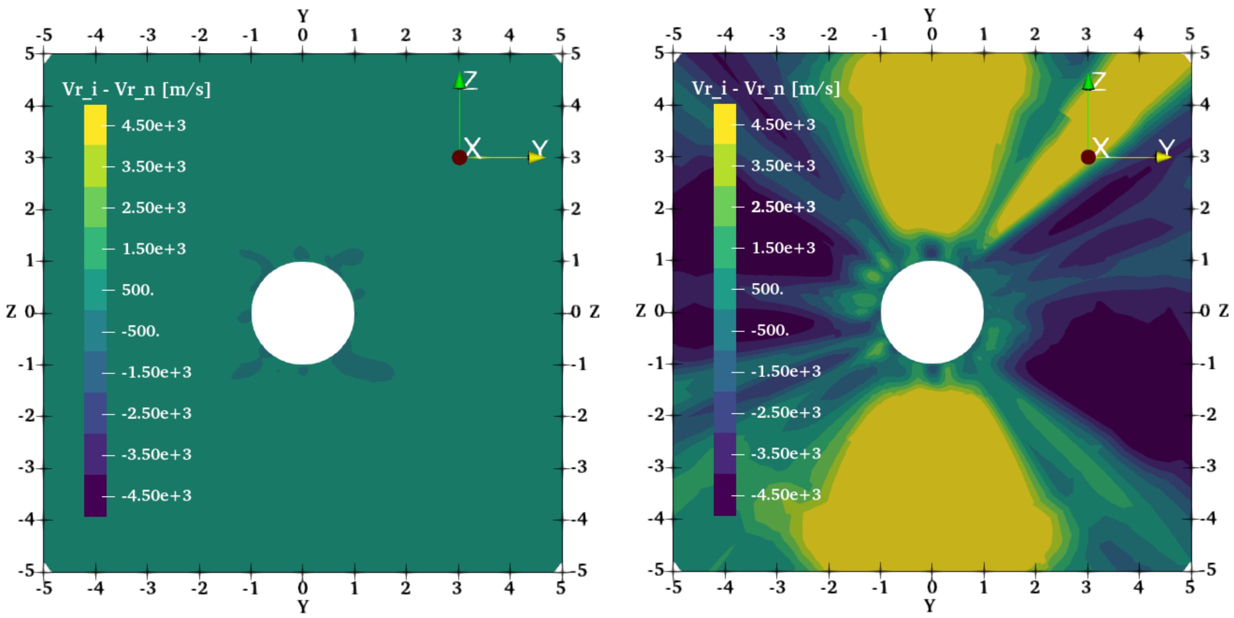

Fig. 6. The contour plots for $V_{\rm i_r} - V_{\rm n_r}$, with (left) and without (right) the source-sink terms in the ion energy equations, in km s^{-1}, corresponding to the case of the solar minimum in *the global model*.

.

conduction, and radiative cooling. For coronal heating, we employed the approach of Mikić et al. (1999), which linked heating to the local magnetic field strength, B, on the premise that regions of stronger magnetic fields were heated more (whether through waves or magnetic reconnection). To incorporate anisotropic thermal conduction, we used the model of Braginskii (1965). Finally, to account for optically thin radiative losses, we added a radiative cooling term, as proposed by Rosner et al. (1978).

Within the framework of the global model, we performed the multi-fluid MHD numerical simulations on realistic data-driven cases to study the corresponding solar minimum (August 1, 2008) and solar maximum (March 9, 2016). In both cases, we compared a model with complete source-sink terms with a baseline model that excluded these terms within the framework of the COCONUT model (Perri et al., 2022, 2023) to understand the dynamics of the solar atmosphere. The developed global model offered new insights into plasma heating, outflows, and their dynamics in the upper solar atmosphere. See Fig. 6 for sample results adopted from Kumar et al. (2026). The results revealed a degree of numerical convergence, and the computational cost remained acceptable, indicating that the multi-fluid MHD model can be effectively utilised in operational space-weather pipelines.

– **Project 6: CME evolution in the corona**

The main objective of Project 6 was to study the evolution of CME flux ropes in the low solar corona. Data-driven modelling, using the photospheric magnetic fields as input, is a common approach to extract information from eruptive coronal magnetic fields (Guo et al., 2024), which, as mentioned earlier, cannot be measured with sufficient accuracy currently. Knowledge of the topology and evolution of potentially eruptive magnetic fields in the solar corona is crucial for space weather forecasting, whether to make initial estimates of their impact on Earth or to constrain various forecasting models (Kilpua et al., 2019).

Project 6 introduced a novel semi-automated tool for extracting CME flux ropes from the modelling data. The underlying method is based on identifying features in maps of quantities, that are related to magnetic flux ropes, such as maps of the magnetic field line twist parameter T_w (see e.g., Berger and Prior, 2006; Liu et al., 2016). The first version of the method, presented in (Wagner et al., 2023), was built on the assumption of a circular cross-section for the flux rope and required that it propagate smoothly across the simulation domain. In (Wagner et al., 2024a), mathematical morphology algorithms (see Project 12) were implemented to relax the restrictive assumptions mentioned above, resulting in notable improvements in extraction results. A Graphical User Interface (GUI) called GUITAR (GUI for Tracking and Analysing flux Ropes) was developed in Wagner et al. (2024c) to make the scheme easier to use and more widely available to the scientific community.

In the publications presenting the extraction tool and GUI, as well as in Wagner et al. (2024b), these new methods were applied to several simulation outputs from data-driven and time-dependent magnetofrictional (MFM) and MHD modelling approaches (Pomoell et al., 2019; Daei et al., 2023) for two particular ARs on the Sun. These applications to real events demonstrated that the extraction algorithm could successfully identify and track eruptive solar flux ropes. These works also provided new insights into the evolution of these eruptive structures: the analysis in (Wagner et al., 2023) demonstrated the complex motion of solar flux rope footpoints in the photo-

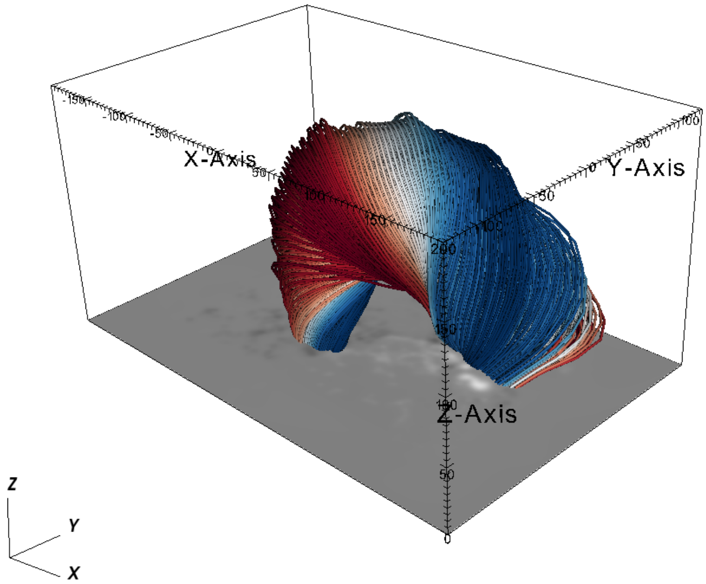

Fig. 7. Flux rope field lines extracted from a time-dependent magnetofrictional simulation of active region AR12473. The vertical magnetic field at the bottom boundary is shown in grayscale, and the spatial (axis) units are Mm.

sphere. The modelled footpoints were further compared to observational data. In particular, it was found that the dynamical evolution of the modelled flux rope footpoints agreed well with the observational estimates derived from chromospheric UV brightenings and coronal EUV dimmings. Applying the updated methodology to AR simulations in (Wagner et al., 2024a) allowed us to follow the flux rope propagation through the lower corona in great detail. This study demonstrated that two flux ropes, with different levels of dynamics, both deflected significantly from their original paths as they rose. Such deflection could have significant implications for space weather forecasts. Interestingly, the extraction algorithm revealed that some eruptive structures may consist of two intertwined flux ropes rather than a single coherent flux rope (Wagner et al., 2024c). Importantly, it was also shown that the distinct twisted flux systems that composed this complex eruption evolved differently. In another study, relaxation simulation runs (i.e., runs where the photospheric driving was stopped at a certain point) were carried out, demonstrating that MFM and MHD approaches exhibit partly different eruptive behaviours. On the one hand, common flux rope properties evolve notably differently, despite the same initial conditions. Moreover, the instabilities of the modelled eruptive systems were investigated, namely the kink instability (see e.g., Török et al., 2004) and the torus instability (see e.g., Kliem and Török, 2006). It was found that the interpretation of which instabilities are responsible for destabilising the flux rope is different, depending on the modelling approach (Wagner et al., 2024b).

– **Project 7: Particle acceleration in coronal shocks**
This project focuses on modelling the acceleration of SEPs in CME-driven shock waves with the particular emphasis on investigating the escape of accelerated particles from the turbulent vicinity of the shock (foreshock region). The general motivation behind this project is the need for

computationally efficient yet accurate numerical models to forecast the characteristics of gradual, CME-associated SEP events across the heliosphere. Numerical models of particle acceleration in shocks, including particle transport effects in large-scale magnetic fields and a fully self-consistent treatment of particle interactions with MHD turbulence, are too computationally heavy to be used in the operational space-weather context. Of great potential for this purpose are hybrid models, where wave-particle interactions are treated self-consistently only in a finite vicinity of the shock, but further away from the shock (toward a distant heliospheric observer), SEPs are propagated as test particles (e.g., Hu et al., 2017). Such models require considerably fewer computational resources. The question arises, however, where in the upstream region, i.e., ahead of the shock, one should place the boundary between these two spatial regions so that fluxes of SEPs escaping from the acceleration region in the hybrid approach agree with the SEP fluxes computed self-consistently everywhere.

A novel hybrid simulation framework, PARASOL, has recently been developed with the ultimate goal of operational space-weather modelling of gradual SEP events (Afanasiev et al., 2025). This framework combines the PARADISE model for the global heliospheric transport of energetic particles and the SOLPACS (SOlar Particle Acceleration in Coronal Shocks; Afanasiev et al., 2015, 2023) model to describe the acceleration of particles in the CME-driven shocks, including the back-reaction of the particles on the Alfvénic turbulence in the upstream region of the shock. SOLPACS uses a finite one-dimensional (1-D) spatial simulation box (to trace particles along a given magnetic field line) with a free-escape upper boundary, i.e., particles that cross this boundary leave the box and do not return. The large-scale magnetic field in the SOLPACS simulation box is assumed homogeneous, so no magnetic focusing is included in the SOLPACS model. In the current version of PARASOL (Afanasiev et al., 2025), the location of the upper free-escape boundary of the SOLPACS simulation box is a free parameter.

To investigate the effect of free-escape boundary position, a 1D Monte Carlo model simulating particle acceleration under simplified coronal conditions has been developed in the project (Annie John et al., 2024). The model uses a constant magnetic focusing length, and the scattering rate in the upstream region is computed using a mean-free-path formulation consistent with the steady-state theory of Bell (1978). Our simulation results (Annie John et al., 2024) demonstrate that the effects of focusing can be mimicked in a simulation without focusing by placing the free-escape boundary ahead of the shock, near the position where particles escape from the shock due to concentration in a simulation with focusing. However, the exact position of the free-escape boundary depends on which particle population (trapped near the shock or escaped from the shock) is addressed.

To move beyond idealised setups, the model developed in the project has been extended by incorporating magnetic field and plasma parameters from the data-driven COCONUT MHD model. The magnetic focusing length was computed via numerical differentiation of the magnetic field magnitude along selected coronal field lines, replacing the simplified assumption of a constant focusing length. Simulations using this extended model show the formation of flat energy spectra of escaped particles (at 1 AU) in the 0.1–2 MeV range, consistent with SEP in-situ observations (Lario et al., 2018; Perri et al., 2023). Additionally, the estimated particle intensities at 1 AU agree well with the observed maximum, known as the streaming-limited intensity levels

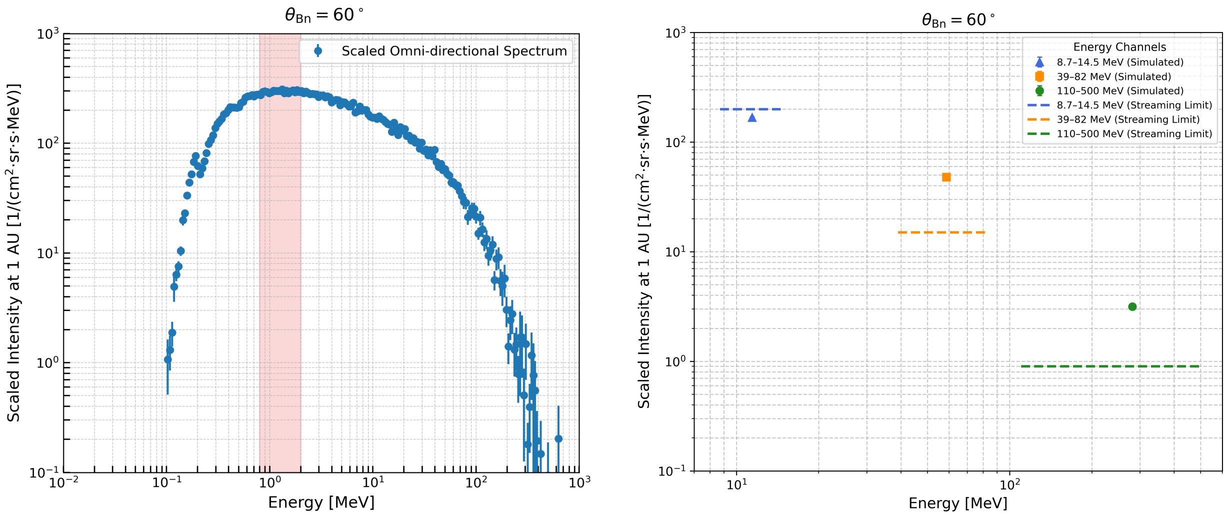

Fig. 8. Simulation results from the particle acceleration model for a quasi-perpendicular shock with $\theta_{Bn} = 60°$. *Left:* Scaled omnidirectional energy spectrum of escaped particles at 1 AU, showing flattening within the 0.1–2 MeV range. *Right:* Corresponding scaled particle intensities at 1 AU compared with the theoretical streaming-limited threshold (Reames and Ng, 1998).

(Reames and Ng, 1998, see Fig. 8). Further work is needed to identify the free-escape boundary position upstream of the shock in such a more realistic setup.

– **Project 8: Particle transport in interplanetary medium**
This project aimed to develop an advanced, focused transport simulation framework capable of modelling SEP events under complex heliospheric conditions. Our starting point was the EUHFORIA-PARADISE model. PARADISE leverages accurate solar wind input from EUHFORIA and solves the focused transport equation (FTE; e.g., van den Berg et al. 2020) in a stochastic manner to propagate energetic particles as test particles through the MHD backgrounds, incorporating nearly all key particle transport processes.

To achieve our goal, we advanced the existing model in three stages. First, we introduced the enhanced Icarus-PARADISE model (Husidic et al., 2024a) by incorporating the Icarus code (Verbeke et al., 2022), which is part of the Message Passing Interface - Adaptive Mesh Refinement Versatile Advection Code (MPI-AMRVAC; Keppens et al. 2012; Xia et al. 2018; Keppens et al. 2023). Similar to EUHFORIA, Icarus is a 3D ideal MHD code that models the global solar wind from 0.1 au onwards, including transient structures such as CMEs and corotating interaction regions (CIRs) containing shocks. Key particle-shock acceleration processes occur on small spatial scales that are challenging to resolve with EUHFORIA; to refine a shock locally, EUHFORIA's uniform, equidistant grid requires global refinement, which is computationally very demanding. Unlike EUHFORIA, MPI-AMRVAC incorporates advanced techniques, including solution-adaptive mesh refinement (AMR) and grid stretching, for more efficient and accurate simulations.

As a first application of the novel code, we conducted a theoretical study of particle acceleration and transport at a CIR (Husidic et al., 2024a). Using a synthetic solar wind setup with embedded

CIRs, we injected protons at the forward and reverse shocks of a CIR and tracked their evolution with PARADISE. We first validated the Icarus-PARADISE model by reproducing the results of the established EUHFORIA-PARADISE model using a uniform Icarus wind. We then assessed the impact of shock resolution by applying various levels of AMR in the shock region within Icarus, which far surpasses the resolution in EUHFORIA. The resulting particle intensity profiles revealed that higher AMR levels consistently led to stronger particle acceleration in the shock regions, highlighting the model's improved capability to resolve shock-related effects.

By modelling CME propagation as well as particle acceleration and transport only from 0.1 au onwards, many critical physical processes already occurring in the corona are ignored, such as the evolution of the CME (Wang et al., 2014), the formation of shocks (Mann et al., 2003), or particle acceleration of SEPs in flare regions or CME-driven shock waves (Reames, 1999; Desai and Giacalone, 2016). Therefore, in the second part of the project, we introduced the novel COCONUT-PARADISE model (Husidic et al., 2024b) to study the evolution of energetic particles in the corona. The global 3D ideal MHD coronal model COCONUT (COOLFluiD COroNal UnsTructured; Perri et al. 2022, 2023; Kuźma et al. 2023) is part of the COOLFluiD (Computational Object-Oriented Libraries for Fluid Dynamics; Lani 2009) platform and generates coronal background configurations, potentially containing CMEs described by the modified analytical Titov–Démoulin magnetic flux rope (MFR) model (Titov and Démoulin, 1999; Titov et al., 2014; Linan et al., 2023).

As a first application, we used COCONUT-PARADISE to study particle transport in the corona in the presence of a CME. We investigated particle confinement in the MFR and the effects of perpendicular diffusion (Husidic et al., 2024b). After generating the coronal backgrounds from 1 to 21.5 $R_\odot$, including an MFR CME, we utilised PARADISE to inject energetic protons inside one of the MFR flanks near its footpoint. We propagated the particles through the coronal backgrounds. Without including the perpendicular diffusion coefficient in the FTE, we found that the particles remained entirely confined to the MFR as it expanded outwards. To model perpendicular diffusion, we employed two approaches: a constant perpendicular Mean Free Path (MFP), a strategy that has often been adopted in heliospheric studies due to its simplicity (e.g., Wijsen et al. 2019; Husidic et al. 2024a); and a model with a gyroradius-dependent perpendicular MFP (e.g., Dröge et al. 2010; Niemela et al. 2024). Using both approaches, we found that relatively small perpendicular MFP lengths—typically used in heliospheric simulations—were already sufficient to produce significant perpendicular diffusion in the corona, both along the CME propagation direction and across longitudes.

Figure 9 shows two snapshots from COCONUT-PARADISE simulations without the application of perpendicular diffusion (panel a) and using the constant perpendicular MFP length ($\lambda_\perp$) approach (Husidic et al., 2024b). The panels display the particle intensities as contours and also contain the Sun with the radial magnetic field component mapped onto it, as well as MFR field lines. Red shades denote positive polarity, blue shades denote negative polarity, and white indicates zero values. The background black field lines are a sample of the global magnetic field. The simulation without perpendicular diffusion (panel a) illustrates how the particles remain confined within the CME, while the snapshot from the simulation with perpendicular diffusion (panel b) shows particles escaping the CME site primarily in the propagation direction, but also longitudinally.

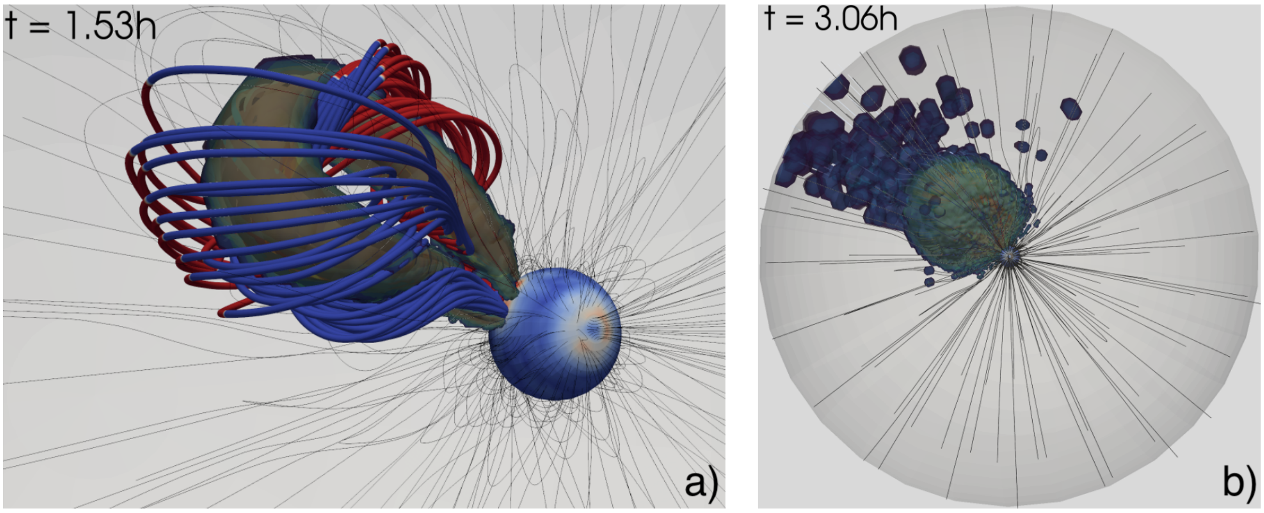

Fig. 9. Proton transport in a coronal CME. Panel a) shows a snapshot of particle intensities as contours from a simulation without applying perpendicular diffusion, together with the MFR and the Sun (with a map of the radial magnetic field component on its surface). The MFR field lines are colour-coded so that red indicates positive polarity, blue indicates negative polarity, and white indicates zero. The black field lines show a sample of the global magnetic field. Panel b) shows a snapshot from a simulation using the constant perpendicular MFP length ($\lambda_\perp$) approach with $\lambda_\perp = 1.075 \times 10^{-2}\,R_\odot$. Adapted from Husidic et al. (2024b).

In space weather research, solar radio bursts play a crucial role, for instance, as precursors to CME-driven shock waves or SEP events (Schwenn, 2006; Klein et al., 2018). Type IV radio bursts are of particular interest due to their potential to infer CME magnetic field strengths from their spectra (Bastian et al., 2001; Maia et al., 2007; Tun and Vourlidas, 2013), but they involve more complex morphology (Pick, 1986) and still-debated emission mechanisms (Morosan et al., 2019). One of the proposed emission mechanisms in type IV bursts is gyrosynchrotron (GS) emission radiated by energetic electrons trapped in CME flux ropes (Dulk, 1973), thereby directly relating the CME's magnetic field strength to the GS emission. Thus, in the third part of the project, we extended the COCONUT-PARADISE model by integrating the Ultimate Fast GS Codes (Fleishman and Kuznetsov, 2010; Kuznetsov and Fleishman, 2021) to the modelling chain (Husidic et al., 2025). In a first study, we simulated the confined propagation of electrons within an MFR CME modelled with COCONUT-PARADISE. We subsequently computed the GS emission spectra generated by the trapped electrons by computing the GS absorption and emission coefficients and solving the radiative transfer equation (see Husidic 2025 for details). By varying CME and electron properties and the observer vantage points, we illustrated their effect on the calculated spectra. We found that GS emission is a key contributor to type IV bursts and that GS emission is strongest in the CME flanks near the footpoints (Husidic et al., 2025).

These advancements of the original EUHFORIA-PARADISE model aim to provide a more realistic modelling of energetic particle acceleration and transport in the heliosphere, to produce valuable information about the evolution of CMEs and SEPs in the corona, and to use this information as further constraints for the heliospheric modelling of CME and SEP events. Furthermore, the coupling of the coronal model COCONUT to PARADISE has also been carried out in anticipation of the coupling of COCONUT to both EUHFORIA (Linan et al., 2025) and Icarus (Baratashvili et al., 2024), allowing, in the future, CME and SEP event simulations from the solar surface to Earth's orbit and beyond.

Project 9: Forecasting CME arrival in the whole heliosphere This project's objective was to provide accurate predictions of CME arrival times at Earth and beyond using statistics-based approaches, leveraging observations from wide-angle viewpoints. Its overarching goal was to extend the capabilities of the Probabilistic Drag-Based Model (P-DBM Napoletano et al., 2018; Del Moro et al., 2019) through a data-driven approach, expanding the model to further extend P-DBM's capabilities approximately 20 AU. A fundamental challenge in implementing the Drag-Based Model (DBM Vršnak et al., 2013; Žic et al., 2015) or its derivatives, such as DBEM (Dumbović et al., 2018; Čalogović et al., 2021) and P-DBM, is the selection of appropriate values for the solar wind speed (ω) and drag efficiency (γ). To address this, the project inferred Probability Distribution Functions (PDFs) for these parameters (ω and γ) from a catalogue of geo-effective CME-Interplanetary CME (ICME) pairs, obtained through the mathematical inversion of the DBM (Mugatwala et al., 2024; Chierichini et al., 2024a). The values of DBM parameters are effectively unknown, and the derived PDFs offer a substantial improvement in predicting ICME arrival times.
Additionally, a significant leap forward has been made to further extend P-DBM's capabilities into the heliosphere. The catalogue of CME–ICME lineup events in Mugatwala et al. (2024) is an outcome towards this goal. This catalogue has highlighted a major limitation of P-DBM, namely that assuming a constant ω is not the best choice; consequently, the value of ω has been estimated over a range of heliocentric distances.
The model has also been validated against existing observations of ICMEs arriving at various locations in the heliosphere. Furthermore, a two-dimensional version of the P-DBM has been developed by incorporating a cone-geometry representation of CMEs. The P-DBM calculations have been refined to account for "Self-Similar-Expansion" (SSE - where the CME maintains its shape during propagation, as in Volpes and Bothmer, 2015) and "Flattening-Cone-Evolution" (FCE - where a geometrical transformation is applied before using the DBM equation on each point of the CME leading edge, considered more realistic, as in Dumbović et al., 2021). See the plot in Figure 10, where a comparison of the propagation for an SSE model and an FCE model is shown for the apex or flank. This implementation of the P-DBM shows competitive Mean Absolute Error (MAE) values in the range of approximately 7 to 11 hours, which is comparable to or slightly better than historical DBM performance and other models (Riley et al., 2018; Vourlidas et al., 2019a). These advancements are then made available through a simple graphical user interface (GUI), representing a practical outcome of this project and transforming the theoretical developments in P-DBM and the compiled datasets into a useful tool for operational space weather forecasting.

– **Project 10: Forecasting solar activity with deep learning**
The overarching goal of Project 10 was to forecast solar activity (specifically flares) within the next 24 to 48 hours using real-time solar images and data. The project leverages the availability of large datasets to train Artificial Neural Networks (ANN, as in Wang et al., 2008; Liu et al., 2019) for classifying solar configurations prone to these activities. Among the results of this project is

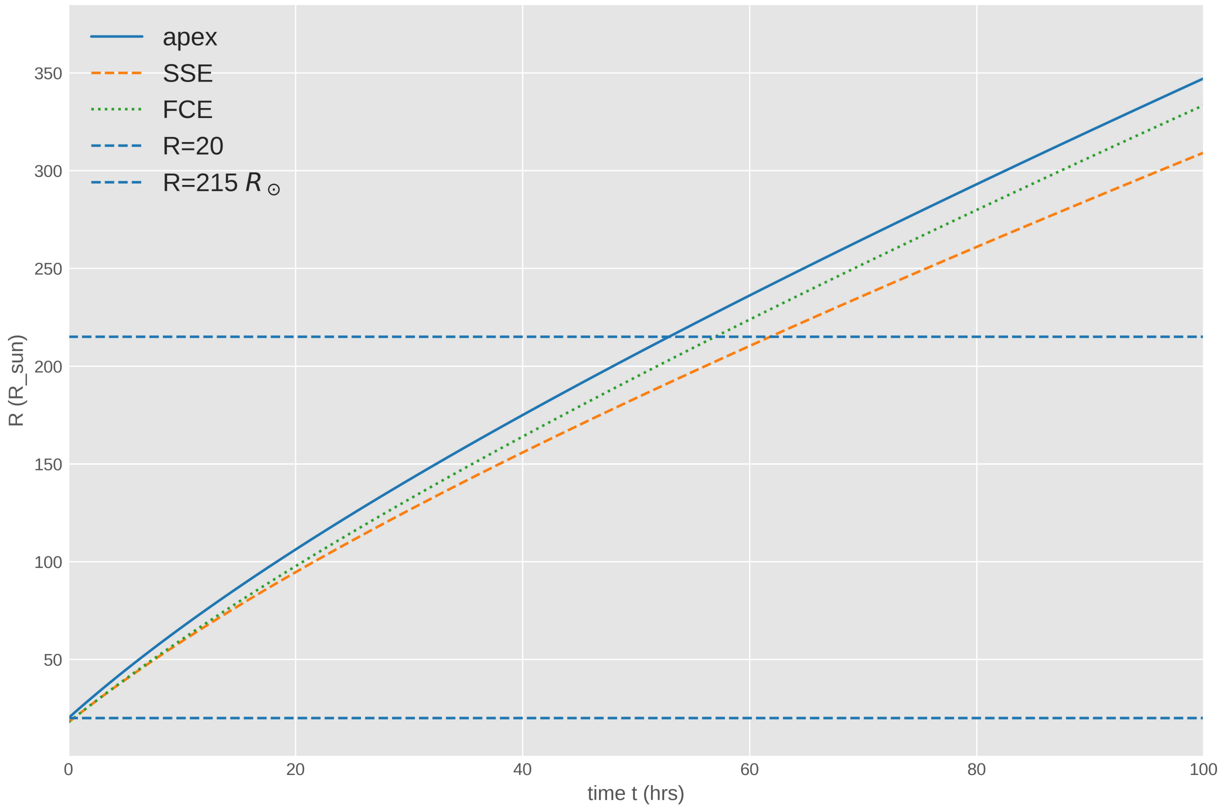

Fig. 10. This figure shows the CME propagation under DBM approximation using ”Self-Similar-Expansion (SSE)” and ”Flattening-Cone-Evolution (FCE)”. CME initial speed v0 = 1000 km/s while DBM parameters are (400 km/s,0.2E-7 km-1). The half angular width of CME ω = 30 and the considered element for the DBM solution is located at 20deg from the apex. From the figure, it is clear that, in FCE, the CME leading edge tends to achieve the same speed as the CME apex before achieving ambient solar wind speed. Also, the figure suggests that at any given heliocentric distance, the speed of any non-apex point on the CME leading edge has a slightly higher speed in the FCE approximation compared to SSE.

the introduction of Patch-distributed Convolutional Neural Networks (P-CNNs Francisco et al., 2025). This framework enables full-disk forecasts while also providing event probabilities in solar subregions and position predictions. This method bypasses challenges associated with unrecorded or misattributed flares that can hinder traditional AR-based machine learning training (Camporeale, 2019). The study employed Grad-CAM analysis (Selvaraju et al., 2017) to explain its predictions, demonstrating that it effectively focused on active regions prone to flaring. The inferred flare positions, derived from the centroid of Grad-CAM intensities within positively classified patches, closely aligned with actual emerging flares, providing operational utility by identifying potential flare locations without reliance on external AR detection (as in Figure 11). Additionally, the same study highlighted how ML models using SDO/AIA Extreme Ultraviolet (EUV) images as inputs (as also done by Leka et al., 2023; Sun et al., 2023) consistently demonstrated improved performance compared to those employing SDO/HMI photospheric magnetograms. Specifically, the C+ coronal model (for predicting whether at least one flare above the

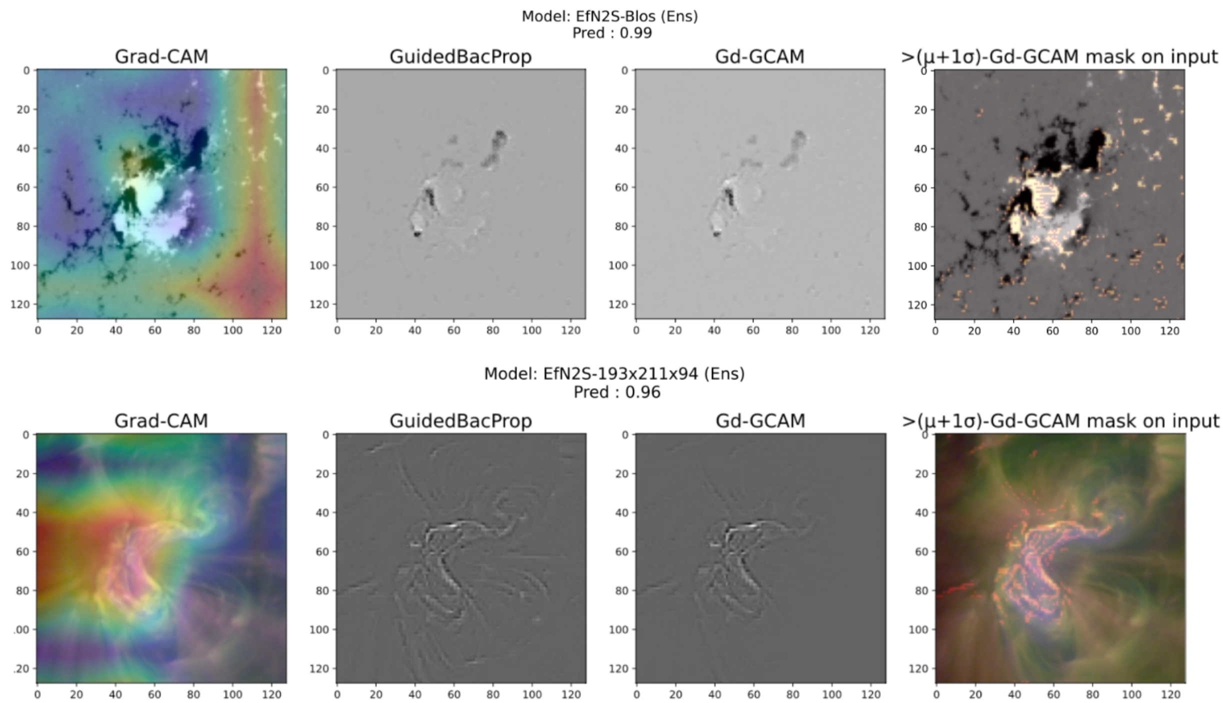

Fig. 11. Explainability results for a C+ flare prediction on AR 12673 the 2017-09-06 few hours prior to an X1.1 flare. The top row displays the results from a magnetogram model, showing that the number of magnetic elements, as well as areas stuck between two elements of opposed polarities, are the strongest contributors to the prediction. The second row displays the results of an EUV model: the prediction appears to come mainly from the sheared coronal loop, exhibiting a clear sigmoidal shape.

C-class threshold will occur in the next 24 hr) achieved a True Skill Statistic (TSS) of 0.74, and the M+ coronal model (predicting at least one flare above the M-class threshold) achieved a TSS of 0.61 on the operational test set, outperforming individual folds. Regarding the use of traditional metrics, the research highlighted that models achieving ”state-of-the-art” performance with conventional metrics, such as TSS and Heidke Skill Score (HSS), may still have limitations. A simple persistence model (predicting the same activity as the previous time window) was found to be surprisingly competitive, sometimes achieving high TSS scores (e.g., >0.70 for C+ and ≈0.45 for M+ Francisco et al., 2025). The study’s deep learning models showed a slight but significant advantage over the persistence model when evaluated using precision-based metrics, such as the Matthews Correlation Coefficient (MCC), HSS, or F1 score. The Persistence Relative F1 (PR-F1) indicates that the deep learning models offered limited improvement over persistence in balancing detection and false alarms. All models demonstrated notably low scores (AC-HSS, AC-TSS, AC-MCC) when evaluated specifically on time windows where solar activity changed (e.g., the first flare after a quiet period or the first quiet period after an active one). This implies that none of the analysed models could predict changes in flaring behaviour significantly better than a random guess. These findings suggest that the learned features are more effective at recognising and classifying ongoing activity or quiet configurations than at anticipating transitions, which is a crucial aspect of practical forecasting. To address the limitations of these standard metrics, this study introduced complementary evaluation methods: the Persistence Relative Skill Scores (PRSS; model performance relative to a persistence baseline) and the Activity-change (AC) and No-change (NC) metrics (separate evaluations of periods of changing versus stable activity).

– **Project 11: CME arrival modelling with Machine Learning**
The goal of this project was to build a fast and accurate engine for predicting the arrival time of CMEs at Earth using ML algorithms. This engine utilizes abundant observational features of past CMEs (such as speed, mass, angular width, position angle, and source region location that can be found in Richardson and Cane, 2010; Yashiro et al., 2004; Mugatwala et al., 2024) and solar wind parameters (including speed, plasma beta, temperature, flow direction, and vector magnetic field as available in the OMNI database [1] - King and Papitashvili, 2005). The project expanded the CME Arrival Time Prediction Using Machine Learning Algorithms (CAT-PUMA Liu et al., 2018) concept, employing supervised learning to gain critical insights into CME arrival at Earth. The study compared various ML models (Support Vector Machines, Random Forest, and XGBoost) for predicting the transit time of CMEs from the Sun to Earth, a regression task. The updated CAT-PUMA, based on an SVM model, achieved the best performance in predicting CME transit time, with an R2 score of 0.80 and an MAE of 7.6 ± 5.2 hours when evaluated using the "best-split validation" (BSV) technique. This randomised hold-out validation method was also the primary evaluation approach used in the original CAT-PUMA model. While this MAE was slightly higher than the original CAT-PUMA, it was measured on a larger test set (Chierichini et al., 2024b). However, when assessed using cross-validation—a more conservative and robust technique—the MAE remained above 10 hours. This suggests that while BSV can yield optimistic performance estimates, such results may not generalise well to new, unseen data, raising concerns about the model's reproducibility. The study also focused on a binary classification task: predicting whether a CME would impact Earth. All models (SVM, Random Forest, XGBoost) showed comparable performance, with accuracy generally exceeding 70%. Due to the highly unbalanced nature of the data (many more non-Earth-impacting CMEs than Earth-impacting ones), the balanced accuracy never exceeded 65%, indicating that while overall accuracy was high, the models struggled with correctly classifying both classes equally. Also, a high false alarm ratio (FAR) of over 70% was observed for Earth-impacting CMEs. This means that while models were good at identifying CMEs that would not impact Earth, they frequently misclassified non-impacting CMEs as potentially impacting Earth. The study employed Shapley values (SHAP - Lundberg and Lee, 2017; Aas et al., 2021) to interpret the models' decision-making processes and identify underlying limitations as shown in Figure 12. For the classification task, SHAP values showed that many misclassified events (false alarms) were heavily influenced by the CME angular width, particularly for halo CMEs (angular width of 360°) that did not actually impact Earth. This suggests the model was primarily confused by the visual characteristic of "halo" CMEs, which are often geoeffective. To overcome these limitations, Chierichini et al. (2024b) suggests incorporating features that better encapsulate key aspects of interplanetary travel (e.g., propagation direction) and additional CME characteristics beyond angular width. They also propose integrating physical information into the model architecture and combining derived features with direct image input (e.g., white-light or EUV images) using ensemble models.

[1] https://omniweb.gsfc.nasa.gov/

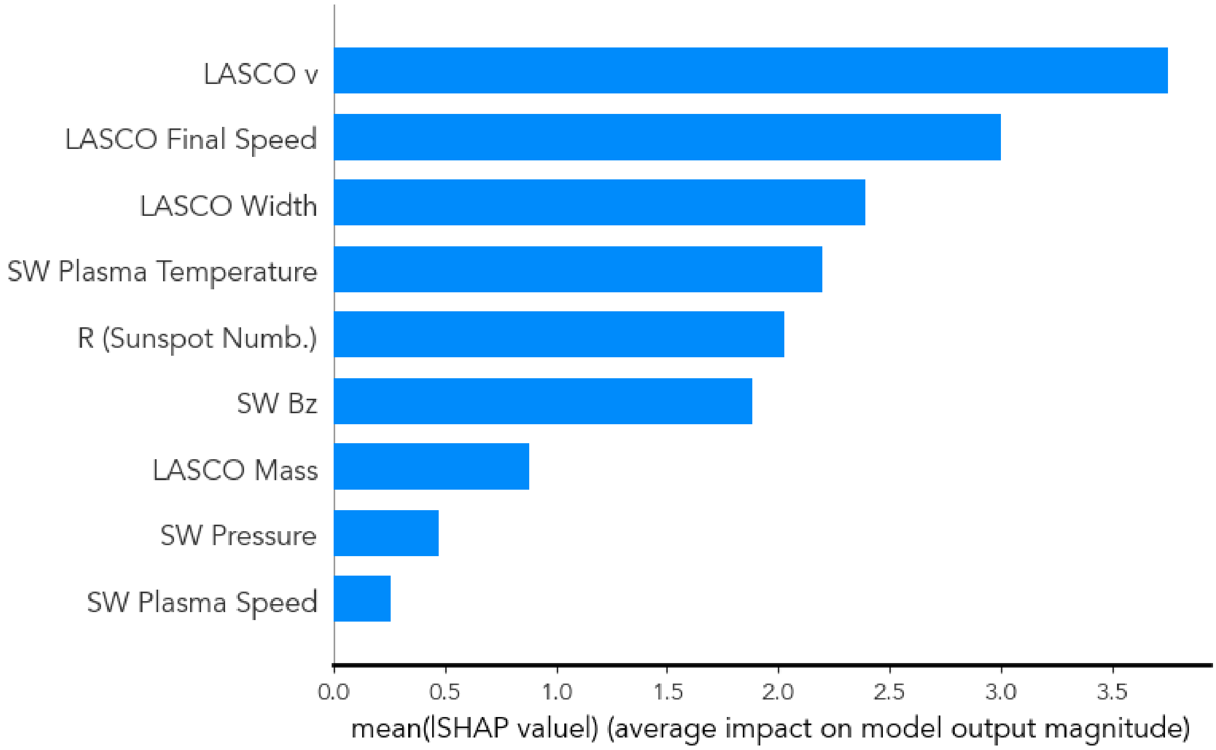

Fig. 12. Mean absolute SHAP values representing the average impact of each feature on the model's output. LASCO v (average CME speed in the LASCO FoV) and LASCO Final Speed are the most influential variables, followed by LASCO Width and solar wind plasma temperature, indicating their dominant role in the model's predictions.

– **Project 12: Development of mathematical morphology algorithms to characterise solar activity.**
The main objective of this project can be summarised in one question: *How can crucial solar surface features from large data sets be effectively identified?* To achieve this goal, we used Mathematical Morphology (MM) to develop algorithms for the automatic extraction of solar characteristics, bearing in mind that the versatility of MM is suitable for dealing with irregular shapes such as sunspots (Hou et al., 2022; Carvalho et al., 2020; Ling et al., 2020; Pucha et al., 2016; Alasta et al., 2018; Zhao et al., 2016; Ravindra et al., 2013; Curto et al., 2008)), active regions (Barata et al., 2018), and filaments (Koch and Rosolowsky, 2015; Hao et al., 2013; Fuller et al., 2005; Shih and Kowalski, 2003), coronal holes (Ciecholewski, 2015; Kirk et al., 2009) and other solar phenomena (Gharat et al., 2023; Stepanyuk et al., 2022; Stenning et al., 2013; Scholl and Habbal, 2008). Another significant advantage of MM is its relative insensitivity to the limb-darkening effect inherent in solar observations or to atmospheric effects in images acquired from ground-based observatories. Thus, in this context, and as part of this project, we explored MM algorithms to detect sunspots (Bourgeois et al., 2024), magnetic flux ropes in collaboration with the SWATNet project 6 (see project 6, Wagner et al. (2024a)), and coronal off-limb structures (Bourgeois et al., 2025).

In relation to sunspots, the MM algorithms were developed to automatically detect sunspot contours in photospheric solar observations. Specifically, the MM algorithm was used to extract sunspots from continuum images acquired with the spectroheliograph at the Geophysical and Astronomical Observatory of the University of Coimbra (OGAUC) and from SDO/HMI intensity images. This approach led to the development of an automated method applicable to images acquired from ground and space missions.

The algorithms were validated quantitatively by comparing the detected sunspot areas with reference values from two established sunspot area databases: the Debrecen Heliophysical Observatory (DHO) (Baranyi et al., 2016) and the Mandal et al. (2020) catalogue. A good agreement was achieved between the values obtained by MM and the areas reported in the catalogues: reaching coefficient correlations of 0.91 MM/DHO and 0.95 MM/Mandal et al. (2020) for corrected sunspot areas, and 0.88 MM/DHO and 0.96 MM/Mandal et al. (2020) projected areas. The methodology details are thoroughly explained in Bourgeois et al. (2024).

The variations in the solar cycle and their evolution can be observed by identifying and tracking solar plasma features, such as coronal off-limb structures, solar jets, coronal loops, and prominences. The project aimed to detect all coronal off-limb structures over a solar cycle and analyse their statistical properties. In particular, to investigate intensity and density evolution of these coronal structures, explicitly focusing on active longitudes in the corona, that is, longitudinal regions where the solar activity is unequivocally dominant. The methodology developed was based on MM algorithms to extract these coronal structures from extreme ultraviolet (EUV) images taken at the 304 Å wavelength channel by the SDO/AIA during Solar Cycle (SC) 24, from June 2010 to December 2021, with a three-hour cadence. This method, described in detail in Bourgeois et al. (2025), and the results enabled the automatic detection of 877,843 coronal-limb structures. Fig. 13 presents an example of the final result of applying the MM algorithm.

The coronal limb structures were analysed for their length, width, area, perimeter, latitude, and longitude (evaluated at the centre of the structures). As a result of most of these properties, similar patterns were observed in the behaviour of the on-disk features, including the butterfly diagram and the structures migrating towards the polar regions (also referred to as 'rush-to-the-poles' structures). Evidence of active longitudes in the corona and their dependence on differential rotation and latitude was found.
The extensive dataset created in this approach has been further exploited in Chierichini et al. (2025) to incorporate MM-derived features (e.g., geometric and morphological descriptors) and enrich a coronal jet dataset, which was subsequently used to train and test a Random Forest ML classification approach that achieved 95% accuracy.

To conclude, within the framework of Project 12, new MM-based algorithms were developed and applied to several solar features. The algorithms robustly identify sunspots and other, more complex and/or irregular structures, enabling extensive statistical studies. The excellent results highlighted MM's potential as a powerful tool for analysing solar images.

3. Other SWATNet activities

The essential principle of SWATNet was to adopt methods that advance scientific progress in space weather and heliophysics, promote interdisciplinary collaboration, and develop diverse research

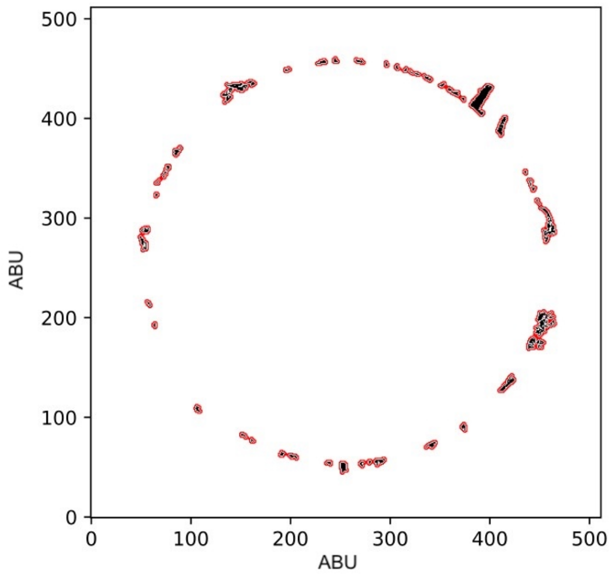

Fig. 13. Contouring of coronal off-limb structures extracted from the image SDO/AIA 304Å image acquired on June 6, 2010, at 15:00:00 UT.

skills valuable in both academic and non-academic environments. To this end, in addition to adopting a new strategy of incorporating learning into a business environment, ESRs were also trained through various schools and workshops on space weather-related topics, as well as other subjects such as Mini MBA, business innovation and entrepreneurship, science communication, and observational training at the Gyula Bay Zoltan Solar Observatory (GSO) operated by the Hungarian Solar Physics Foundation (HSPF. Industrial training was an additional, integral, and significant component of the SWATNet project. It was designed to provide ESRs with practical skills and exposure to non-academic environments. All SWATNet ESRs were required to spend at least one month working with one or more non-academic Partner Organisations. In addition, each ESR had a non-academic mentor who provided support and assistance with networking within companies and the industry, as well as with career planning beyond the secondments. The Partner Organisations contributed to the training program by offering diverse opportunities and materials, including seminars and tutorials at SWATNet workshops and summer schools, and by participating in outreach activities. In addition to their industrial secondments, each student undertook a one-month observational training programme at GSO/HSPF. The observatory also serves as the headquarter of the Solar Activity Monitor Network (SAMNet). During the observational training programme, students gained hands-on experience with the onsite solar telescope equipped with a magneto-optical filter (MOF) – an advanced instrument capable of measuring Doppler velocity and magnetic field strength in the solar chromosphere (Erdélyi et al., 2022). These observations are essential for monitoring solar activity and improving forecasts of solar flares and CMEs. SWATNet was strongly committed to disseminating scientific results. All ESRs presented their findings at national and international conferences and meetings, including the European Space Weather Week, COSPAR, the EGU General Assembly, the American Geophysical Union (AGU) Fall Meeting, and the final SWATNet network conference. SWATNet collectively engaged in STEM Discovery Campaign [2](SDC) activities and the Horizon Results Booster [3] (HRB) program to enhance its visibility within the scientific community and the general public. The SDC is a collaborative international project by Scientix, Europe's largest science education network. It aims to foster collaboration among STEM educators, researchers, policymakers, and stakeholders, inspiring students to pursue careers in STEM fields. The HBR project, initiated by the European Commission (EC), aims to maximise the use of publicly funded research within the EC. The initiative focuses on collaborative dissemination activities, strengthening existing collaborations, establishing new partnerships, and refining dissemination skills. SWATNet joined the HRB and, in collaboration with similar EU projects—SERPENTINE, IDOLS, SOLER, and SPEARHEAD—created the Space Weather Cluster. SWATNet has actively fostered connections within social media by maintaining a vibrant presence across multiple platforms. This engagement is facilitated through the SWATNet blog [4], social media interactions on X [5], professional networking on LinkedIn [6], and informative e-newsletters [7] readily accessible on the project's page. The individual activities of both the partners and the ESRs included science festivals, communications to the media (newspapers, interviews, and radio), public talks, and the European Researchers' Night, in which the SWATNet ESRs and researchers participated in multiple editions throughout the project. These initiatives enabled SWATNet to disseminate valuable knowledge and actively engage a broader audience. This strategic approach significantly amplified its impact on the community and fostered stronger, more collaborative links between the consortium members.

4. Conclusions

This paper summarises the diverse achievements of the Marie Curie ITN project SWATNet, active from 1 March 2021 to 30 August 2025. The project brought together ten academic institutions and five industry partners to train twelve PhD students in space weather and heliophysics.

1. **Science**: SWATNet significantly advanced the understanding of space weather drivers through coordinated, interdisciplinary research across solar and heliospheric domains. Key scientific achievements include significant advancements in modelling and empirical proxies for solar eruptions, enhanced modelling of the corona and particle propagation and transport, improved predictive capabilities, and insights into solar cycle variability through dynamo modelling and the use of extended observational datasets. Research methods focused on incorporating interdisciplinary techniques, such as AI/ML and image processing, as well as various numerical modelling approaches. Research conducted across multiple SWATNet projects resulted in the publication of 26 articles in peer-reviewed journals, all of which acknowledge SWATNet funding. Additionally, several presentations, oral and/or posters, were presented at international conferences.

2. **Collaborative outcomes**: SWATNet was designed as a unique doctoral programme that combines research training and transferable skills with multiple placements, including training at

[2] https://scientix.eu/events/campaigns/sdc22/
[3] https://www.horizonresultsbooster.eu/
[4] https://swatnet.eu/blog/
[5] https://x.com/SWATNetProject
[6] https://www.linkedin.com/groups/12623482/
[7] https://swatnet.eu/communication/e-newsletter/

observatories and industrial exposure. Based on 12 scientific projects, expectations were exceeded, as the ERs leveraged partnerships, resulting in strong, unique scientific collaboration between students and supervisors. Building on these foundations, research conducted within the SWATNet network produced significant contributions across multiple projects that would not have been achievable in isolated doctoral programmes. A central dimension of this collaborative environment was the continuous cross-exposure among projects. ESRs working on machine learning-based flare forecasting attended the same schools and workshops as colleagues developing MHD coronal models or particle transport codes. Those focused on CME arrival prediction were exposed to the physical modelling perspectives of peers working on flux rope evolution and magnetic helicity budgets. This shaped methodological choices, prompted new scientific questions, and fostered a systems-level understanding of the Sun-to-Earth chain that no single project could have instilled on its own. In this sense, the network functioned as more than the sum of its parts: the simultaneous coexistence of 12 projects within a shared training environment was itself a scientific and educational resource. These dynamics are reflected concretely in the research outcomes. In projects 1 to 4, new proxies utilising transient coronal brightening and three-dimensional magnetic reconstructions were developed to differentiate eruptive from non-eruptive active regions, thereby enabling early warnings for solar eruptions (projects 1 and 3). Project 2 introduced a refined methodology for estimating the near-Sun magnetic field strength of CMEs by applying the source helicity budget and integrating advanced near-Sun modelling with inner-heliospheric CME propagation models. Project 4 improved the source terms in surface flux transport models, which enhanced the accuracy of solar cycle forecasting, placing the short-term forecasting efforts in a long-term context. Further integrating project outcomes, projects 5 to 8 were interconnected through a shared modelling framework and several common models. The COCONUT model, in particular, was implemented in projects 5, 7, and 8. Due to the simultaneous progression of these projects, a sequential development approach, such as moving from MHD to SEP modelling, was not possible. Consequently, Projects 7 and 8 pursued distinct methodologies: one advanced understanding of the fundamental processes that influence particle acceleration in the corona, while the other focused on multidimensional transport in the corona and the solar wind. Collectively, these efforts contributed to a deeper understanding of solar eruptive processes and their effects on the space environment. Finally, within project 12, collaborations with projects 6 and 11 sparked innovative solutions. In project 6, a morphological algorithm was developed to extract flux ropes from simulation images across diverse locations, dates, and relaxation times, unveiling new insights. For project 11, the goal was to create a robust database of coronal jets, paving the way for effective training of machine learning algorithms.

3. **Other activities**: Beyond scientific research, SWATNet provided ESRs with comprehensive training encompassing technical, transferable, and core research skills. Industrial secondments, practical observatory training, SWATNet training activities, including three schools and seven workshops, as well as outreach activities and frequent conference participation, allowed students to build strong skill sets and broaden their career opportunities. Industrial training, along with academic training and international exposure, significantly enhanced the career perspectives and job competence of ESRs in both academic and non-academic sectors. It enabled the ESRs to strengthen their network through connections across various sectors; to gain a solid understanding of tasks in different professional contexts; to acquire valuable practical skills and contacts

often lacking in traditional doctoral training programs; and ultimately to be highly competitive for jobs in sectors related to space weather applications, science communication, and the growing space industry (e.g., nano- and microsatellite sectors).

4. **Lessons learned**: SWATNet was a transformative experience for all parties involved. Working within the same broad, cutting-edge theme was motivating for both the ESRs and their supervisors and enhanced the network's scientific impact. Careful planning and the early adoption of effective working methods were essential to ensure the timely completion of the ambitious training programme. The training activities—such as schools and workshops—benefited greatly from diverse formats, including hands-on sessions and pitch talks, which provided ESRs with real-world experience. Involving the broader scientific community further enhanced networking opportunities. The industrial secondments and practical observatory training, while time-consuming, had a clearly positive impact on the students. To maximise their benefits without affecting the progress on the PhD work, we deemed it useful for the ESRs to experience industrial exposure toward the end of the project, when students have already produced most of their scientific results and acquired a solid understanding. Key factors behind the high-quality scientific output included the dedication of both supervisors and ESRs, as well as collaboration among the researchers, which clearly enhanced their productivity. The emphasis on interdisciplinary methods, applicable across a range of fields, proved a useful strategy for expanding students' employability. While Marie Curie ITNs are administratively complex projects and demand strong management, including continuous institutional support, they are also highly rewarding, offering substantial benefits to researchers, institutions, and the broader scientific community. The bureaucratic aspects of SWATNet were also challenges that were successfully learned and overcome. Examples include the modus operandi of each university, in accordance with the laws of each country, which sometimes complicates processes, such as logistics related to joint or double degrees. Another aspect is the need to facilitate the logistics for selected students from outside the EU, including residence permits and related matters. The involvement of a project manager was also essential, as it allowed for addressing risks such as project delays, budget overruns, and insufficient communication. With a dedicated project manager, the coordinator received constant support in managing administrative and communication aspects, as well as in supporting WP leaders, individual partners, and PhD students. It was essential for SWATNet, particularly during the COVID pandemic.

Acknowledgements. The SWATNet consortium expresses its gratitude for the continuous support received from VaBo Consult [8] and its representative, who served as the project support manager.

Funding. This work was supported by the European Union's Horizon 2020 research and innovation programme under the Marie Skłodowska-Curie grant agreement No 955620. The authors would also like to thank the Horizon Results Booster programme, which is supported by the European Union. MBK is grateful for the Leverhulme Trust Found ECF-2023-271. RE is grateful to STFC (UK, grant number ST/M000826/1) and PIFI (China, grant number No. 2024PVA0043). This work was also supported by the NKFIH Excellence Grant TKP2021-NKTA-64. RE and MBK also thank for the support received from NKFIH OTKA (Hungary, grant No. K142987). MBK, RE and MG acknowledge support from ISSI-BJ ("Step forward in solar flare and coronal mass ejection (CME) predicting"). TB and RG would like to thanks to Fundação para a Ciência e a Tecnologia (FCT) through the research grants UIDB/04434/2020 (DOI:

[8] https://www.vaboconsult.com

10.54499/UIDB/04434/2020), UIDP/04434/2020.FCT (DOI: 10.54499/UIDP/04434/2020) and JF through the research grants UIDP/00611/2025 and UIDB/00611/2025. DDM, SC and RM acknowledge the support of the project COronal mass ejection, solar eNERgetic particle and flare forecaSTing from phOtospheric sigNaturEs (CORNERSTONE), funded under the National Recovery and Resilience Plan (NRRP), Missione 4 "Istruzione e Ricerca" – Componente C2 – Investimento 1.1, "Fondo per il Programma Nazionale di Ricerca e Progetti di Rilevante Interesse Nazionale (PRIN)" – Call for tender No. 1409 of 14/09/2022 of the Italian Ministry of University and Research, funded by the European Union – NextGenerationEU Award Number: P2022RKXH9. Computational resources and services used in project 8 were provided by the VSC (Flemish Supercomputer Centre), funded by the Research Foundation - Flanders (FWO) and the Flemish Government, Department EWI. SP is funded by the European Union (ERC-AdG agreement No 101141362, Open SESAME). Views and opinions expressed are, however, those of the author(s) only and do not necessarily reflect those of the European Union or the European Research Council. Neither the European Union nor the granting authority can be held responsible for them. SP is also funded by the projects C16/24/010 (C1 project Internal Funds KU Leuven), G0B5823N and G002523N (WEAVE) (FWO-Vlaanderen), and 4000145223 (SIDC Data Exploitation (SIDEX2), ESA Prodex).

Conflict of Interest. The authors declare no Conflict of Interest.

Data Availability. The raw data availability described in this paper can be found on each respective source identified on the manuscript.

References

Aas, K., M. Jullum, and A. Løland, 2021. Explaining individual predictions when features are dependent: More accurate approximations to Shapley values. *Artificial Intelligence*, **298**, 103,502. https://doi.org/10.1016/j.artint.2021.103502. 2

Afanasiev, A., M. Battarbee, and R. Vainio, 2015. Self-consistent Monte Carlo simulations of proton acceleration in coronal shocks: Effect of anisotropic pitch-angle scattering of particles. *Astron Astrophys*, **584**, A81. https://doi.org/10.1051/0004-6361/201526750, 1603.08857. 2

Afanasiev, A., R. Vainio, D. Trotta, S. Nyberg, N. Talebpour Sheshvan, H. Hietala, and N. Dresing, 2023. Self-consistent modeling of the energetic storm particle event of November 10, 2012. *Astrophys J*, **679**, A111. https://doi.org/10.1051/0004-6361/202346220, 2310.00993. 2

Afanasiev, A., N. Wijsen, and R. Vainio, 2025. Towards advanced forecasting of solar energetic particle events with the PARASOL model. *J Space Weather Space Clim*, **15**, 3. https://doi.org/10.1051/swsc/2024039, 2412.11852. 2

Alasta, A., A. Algamudi, R. Qahwaji, and S. Ipson, 2018. Identification of Sunspots on SODISM Full-Disk Solar Images. *J Multi Proc Tech*, **9**, 3. http://dx.doi.org/10.1051/swsc/2015000. 2

Alissandrakis, C. E., 1981. On the computation of constant alpha force-free magnetic field. *Astron Astrophys*, **100**(1), 197–200. 2

Annie John, L., S. Nyberg, L. Vuorinen, R. Vainio, A. Afanasiev, S. Poedts, and N. Wijsen, 2024. Effects of Adiabatic Focusing and Free-Escape Boundaries in Coronal Shock Acceleration. *J Space Weather Space Clim*, **14**, 15. https://doi.org/10.1051/swsc/2024012. 2

Bamba, Y., K.-S. Lee, S. Imada, and K. Kusano, 2017. Study on Precursor Activity of the X1.6 Flare in the Great AR 12192 with SDO, IRIS, and Hinode. *Astrophys J*, **840**(2), 116. Publisher: American Astronomical Society, https://iopscience.iop.org/article/10.3847/1538-4357/aa6dfe. 2

Bamba, Y., T. T. Yamamoto, and T. J. Okamoto, 2013. Sudy on the triggering process of solar flares based on *HINODE*/SOT observations. *Astrophys J*, **778**(1), 48. Publisher: American Astronomical Society, https://doi.org/10.1088/0004-637x/778/1/48. 2

Baranyi, T., L. Gyõri, and A.Ludmány, 2016. Heritage of Konkoly's solar observations: the Debrecen photoheliograph programme and the Debrecen sunspot databases. *Conference dedicated to the 100th anniversary of the death of Dr. Nicolaus Thege-Konkoly*, A31. https://arxiv.org/abs/1608.08419. 2

Barata, T., S. Carvalho, I. Dorotovič, F. P. A. Garcia, J. Fernandes, and A. M. Lourenço, 2018. Software tool for automatic detection of solar plages in the Coimbra Observatory spectroheliograms. *Astron Comp*, **24**, 70–83. http://dx.doi.org/10.1051/swsc/2015000. 2

Baratashvili, T., M. Brchnelova, L. Linan, A. Lani, and S. Poedts, 2024. The operationally ready full 3D magnetohydrodynamic model from the Sun to Earth: COCONUT+Icarus. *Astron Astrophys*, **690**, A184. https://doi.org/10.1051/0004-6361/202449389. 2

Bastian, T. S., M. Pick, A. Kerdraon, D. Maia, and A. Vourlidas, 2001. The Coronal Mass Ejection of 1998 April 20: Direct Imaging at Radio Wavelengths. *Astrophys J*, **558**, L65. https://iopscience.iop.org/article/10.1086/323421. 2

Bell, A. R., 1978. The acceleration of cosmic rays in shock fronts - I. *Mon Notices Royal Astron Soc*, **182**, 147–156. 10.1093/mnras/182.2.147. 2

Benz, A. O., 2017. Flare Observations. *Living Rev Sol Phys*, **14**(1), 2. https://doi.org/10.1007/s41116-016-0004-3. 1.2

Berger, M. A., and C. Prior, 2006. The writhe of open and closed curves. *J of Phys Math General*, **39**(26), 8321–8348. https://doi.org/10.1088/0305-4470/39/26/005. 2

Biswal, S., M. B. Korsós, M. K. Georgoulis, A. Nindos, S. Patsourakos, and R. Erdélyi, 2024. Case Studies on Pre-eruptive X-class Flares using R-value in the Lower Solar Atmosphere. *Astrophys J*, **974**(2), 259. https://dx.doi.org/10.3847/1538-4357/ad6c33. 3, 2

Bobra, M. G., and S. Couvidat, 2015. Solar Flare prediction using SDO/HMI vector magnetic field data with a Machine-Learning algorithm. *Astrophys J*, **798**(2), 135. https://doi.org/10.1088/0004-637X/798/2/135. 2

Bobra, M. G., and S. Ilonidis, 2016. Predicting Coronal Mass Ejection using Machine Learning methods. *Astrophys J*, **821**(2), 127. https://doi.org/10.3847/0004-637X/821/2/127. 2

Bothmer, V., and R. Schwenn, 1998. The structure and origin of magnetic clouds in the solar wind. *Annales Geophysicae*, **16**(1), 1–24. https://doi.org/10.1007/s00585-997-0001-x. 2

Bourgeois, S., T. Barata, R. Erdélyi, R. Gafeira, and O. Oliveira, 2024. Sunspots Identification Through Mathematical Morphology. *Sol Phys*, **299**, 21. https://doi.org/10.1007/s11207-023-02243-1. 2

Bourgeois, S., S. Chierichini, S. Soós, R. Erdélyi, J. Liu, M. B. Korsós, R. Gafeira, and T. Barata, 2025. Long-term properties of coronal off-limb structures. *Astron Astrophys*, **693**, A301. https://DOI:10.1051/0004-6361/202451257. 2

Braginskii, S. I., 1965. Transport Processes in a Plasma. *Rev Plasma Phy*, **1**, 205. 2

Čalogović, J., M. Dumbović, D. Sudar, B. Vršnak, K. Martinić, M. Temmer, and A. M. Veronig, 2021. Probabilistic drag-based ensemble model (DBEM) evaluation for heliospheric propagation of CMEs. *Sol Phys*, **296**(7), 114. https://doi.org/10.1007/s11207-021-01859-5. 2

Camporeale, E., 2019. The challenge of machine learning in space weather: Nowcasting and forecasting. *Space weather*, **17**(8), 1166–1207. https://doi.org/10.1029/2018SW002061. 2

Camporeale, E., 2019. The Challenge of Machine Learning in Space Weather: Nowcasting and Forecasting. *Space Weather*, **17**(8), 1166–1207. https://doi.org/10.1029/, 1903.05192. 1.1

Carvalho, S., S. Gomes, T. Barata, A. Lourenço, and N. Peixinho, 2020. Comparison of automatic methods to detect sunspots in the Coimbra Observatory spectroheliograms. *Astron Comp*, **32**, 19. https://doi.org/10.1016/j.ascom.2020.100385. 2

Chen, H., J. Zhang, L. Li, and S. Ma, 2016. Tether-Cutting reconnection between two solar filaments triggering outflows and a Coronal Mass Ejection. *Astrophysical J letters*, **818**(2), L27. https://iopscience.iop.org/article/10.3847/2041-8205/818/2/L27. 2

Chierichini, S., S. Bourgeois, S. Soós, J. Liu, M. Korsós, D. Del Moro, and R. Erdélyi, 2025. Coronal jet Identification with machine learning. *Astron Astrophys*, **698**, A50. https://doi.org/10.1051/0004-6361/202452312. 2

Chierichini, S., G. Francisco, R. Mugatwala, R. Foldes, E. Camporeale, G. De Gasperis, L. Giovannelli, G. Napoletano, D. Del Moro, and R. Erdelyi, 2024a. A Bayesian approach to the drag-based modelling of ICMEs. *J Space Weather Space Clim*, **14**, 1. https://doi.org/10.1051/swsc/2023032. 2

Chierichini, S., J. Liu, M. B. Korsós, D. Del Moro, and R. Erdélyi, 2024b. CME arrival modeling with machine learning. *Astrophys J*, **963**(2), 121. DOI10.3847/1538-4357/ad1cee. 2, 2

Chifor, C., D. Tripathi, H. E. Mason, and B. R. Dennis, 2007. X-ray precursors to flares and filament eruptions. *Astron Astrophys*, **472**(3), 967–979. Publisher: EDP Sciences, 10.1051/0004-6361:20077771, URL http://www.aanda.org/10.1051/0004-6361:20077771. 2

Ciecholewski, M., 2015. Automated coronal hole segmentation from Solar EUV Images using the watershed transform. *J Vis Comm Image Rep*, **33**, 203–218. https://doi.org/10.1016/j.jvcir.2015.09.015. 2

Curto, J., M. Blanca, and E. J. Martinez, 2008. Automatic sunspots detection on full–disk solar images using mathematical morphology. *Sol Phys*, **250**, 411–429. https://doi.org/10.1007/s11207-008-9224-6. 2

Daei, F., J. Pomoell, D. J. Price, A. Kumari, S. Good, and E. K. J. Kilpua, 2023. Modeling the formation and eruption of coronal structures by linking data-driven magnetofrictional and MHD simulations for AR 12673. *Astron Astrophys*, **676**, A141. https://doi.org/10.1051/0004-6361/202346183. 2

Del Moro, D., G. Napoletano, R. Forte, L. Giovannelli, E. Pietropaolo, and F. Berrilli, 2019. Forecasting the 2018 February 12th CME propagation with the P-DBM model: A fast warning procedure. *Annals of Geophysics*, **62**(4), GM456–GM456. https://doi.org/10.4401/ag-7750. 2

Demoulin, P., and S. Dasso, 2009. Causes and consequences of magnetic cloud expansion. *Astron Astrophys*, **498**. 10.1051/0004-6361/200810971. 2

Desai, M., and J. Giacalone, 2016. Large gradual solar energetic particle events. *Living Rev Sol Phys*, **13**(1), 3. https://doi.org/10.1007/s41116-016-0002-5. 2

Dissauer, K., G. Barnes, K. D. Leka, and E. L. Wagner, 2025. On the Uniqueness and Causal Relationship of Precursor Activity to Solar Energetic Events: I. Transient Brightenings – Introduction and Overview. ArXiv:2503.12338 [astro-ph], 10.3847/1538-4357/adbf13. 2

Dissauer, K., K. D. Leka, and E. L. Wagner, 2023. Properties of Flare-imminent versus Flare-quiet Active Regions from the Chromosphere through the Corona. I. Introduction of the AIA Active Region Patches (AARPs). *Astrophys J*, **942**(2), 83. 10.3847/1538-4357/ac9c06. 2

Dröge, W., Y. Y. Kartavykh, B. Klecker, and G. A. Kovaltsov, 2010. Anisotropic Three-Dimensional Focused Transport of Solar Energetic Particles in the Inner Heliosphere. *Astrophys J*, **709**(2), 912–919. https://doi.org/10.1088/0004-637X/709/2/912. 2

Dulk, G. A., 1973. The Gyro-Synchrotron Radiation from Moving Type IV Sources in the Solar Corona. *Sol Phys*, **32**, 491. https://doi.org/10.1007/BF00154962. 2

Dumbović, M., J. Čalogović, K. Martinić, B. Vršnak, D. Sudar, M. Temmer, and A. Veronig, 2021. Drag-based model (DBM) tools for forecast of coronal mass ejection arrival time and speed. *Frontiers Astron Space Sci*, **8**, 639,986. https://doi.org/10.3389/fspas.2021.639986. 2

Dumbović, M., J. Čalogović, B. Vršnak, M. Temmer, M. L. Mays, A. Veronig, and I. Piantschitsch, 2018. The drag-based ensemble model (DBEM) for coronal mass ejection propagation. *Astrophys J*, **854**(2), 180. https://doi.org/1538-4357/aaaa66. 2

Eastwood, J. P., E. Biffis, M. A. Hapgood, L. Green, M. M. Bisi, R. D. Bentley, R. Wicks, L. A. McKinnell, M. Gibbs, and C. Burnett, 2017. The Economic Impact of Space Weather: Where Do We Stand? *Risk Analysis*, **37**(2), 206–218. https://doi.org/10.1111/risa.12765. 1

Erdélyi, R., M. B. Korsós, X. Huang, Y. Yang, D. Pizzey, et al., 2022. The Solar Activity Monitor Network - SAMNet. *J Space Weather Space Clim*, **12**, 2. https://doi.org/10.1051/swsc/2021025. 3

Farrugia, C. J., M. Leiter, H. K. Biernat, R. Schwenn, K. W. Ogilvie, H. Matsuil, H. Kucharek, V. K. Jordanova, and R. P. Lepping, 2005. Evolution of Interplanetary Magnetic Clouds from 0.3 AU to 1 AU: A Joint Helios-Wind Investigation. In B. Fleck, T. H. Zurbuchen, and H. Lacoste, eds., Solar Wind 11/SOHO 16, Connecting Sun and Heliosphere, vol. 592 of *ESA Special Publication*, 723. 2

Fleishman, G. D., and A. A. Kuznetsov, 2010. Fast Gyrosynchrotron Codes. *Astrophys J*, **721**, 1127. DOI10.1088/0004-637X/721/2/1127. 2

Francisco, G., M. Berretti, S. Chierichini, R. Mugatwala, J. M. Fernandes, T. Barata, and D. Del Moro, 2025. Limits of solar flare forecasting models and new deep learning approach. *Astrophys J*, **985**(1), 10. DOI10.3847/1538-4357/adc56d. 2, 2

Fuller, N., J. Aboudarhma, and R. Bentley, 2005. Filament recognition and image cleaning on meudonH-alpha spectroheliograms. *Sol Phys*, **227**, 61–73. https://doi.org/10.1007/s11207-005-8364-1. 2

Georgoulis, M. K., K. Tziotziou, and N.-E. Raouafi, 2012. Magnetic energy and helicity budgets in the active-region solar corona. II. Nonlinear force-free approximation. *Astrophys J*, **759**(1), 1. https://dx.doi.org/10.1088/0004-637X/759/1/1. 2

Georgoulis, M. K., S. L. Yardley, J. A. Guerra, S. A. Murray, A. Ahmadzadeh, et al., 2024. Prediction of solar energetic events impacting space weather conditions. *Adv Space Res*. https://doi.org/10.1016/j.asr.2024.02.030. 2

Gharat, S., B. Bose, A. Borthakur, and R. Mazumder, 2023. An image processing approach to identify solar plages observed at 393.37 nm by the Kodaikanal solar observatory. *RAS Techniques and Instruments*, **2**, 393–397. https://doi.org/10.1093/rasti/rzad027. 2

Good, S. W., E. K. J. Kilpua, A. T. LaMoury, R. J. Forsyth, J. P. Eastwood, and C. Möstl, 2019. Self-Similarity of ICME Flux Ropes: Observations by Radially Aligned Spacecraft in the Inner Heliosphere. *J Geophys Res: Space Phys*, **124**(7), 4960–4982. https://doi.org/10.1029/2019JA026475, 1905.07227. 2

Guo, Y., J. Guo, Y. Ni, C. Xia, Z. Zhong, M. Ding, P. Chen, and R. Keppens, 2024. Magnetic flux rope models and data-driven magnetohydrodynamic simulations of solar eruptions. *Rev of Mod Plasma Phys*, **8**(1), 29. https://doi.org/10.1007/s41614-024-00167-2. 2

Hao, Q., C. Fang, and P. F. Chen, 2013. Developing an advanced automated method for solar filament recognition and its scientific application to a solar cycle of MLSO Halpha data. *Sol Phys*, **286**, 385–404. https://doi.org/10.1007/s11207-013-0285-9. 2

Hou, J., S. Zeng, S. Zheng, X. Luo, L. Deng, Y. Li, Y. Chen, G. Lin, Y. Feng, and J. Tao, 2022. Chinese Sunspot Drawings and Their Digitization—(VII) Sunspot Penumbra to Umbra Area Ratio Using the Hand-Drawing Records from Yunnan Observatories. *Res Astron Astrophys*, **22**, 8. https://doi.org/10.1088/1674-4527/ac7f87. 2

Hu, J., G. Li, X. Ao, G. P. Zank, and O. Verkhoglyadova, 2017. Modeling Particle Acceleration and Transport at a 2-D CME-Driven Shock. *J Geophys Res: Space Phys*, **122**(11), 10,938–10,963. https://doi.org/10.1002/2017JA024077. 2

Husidic, E., 2025. Multi-scale modelling of energetic particle dynamics and radio signatures in coronal and heliospheric plasmas. Ph.D. thesis, KU Leuven/University of Turku. 2

Husidic, E., N. Wijsen, T. Baratashvili, S. Poedts, and R. Vainio, 2024a. Energetic particle acceleration and transport with the novel Icarus + PARADISE model. *J Space Weather Space Clim*, **14**, 11. https://doi.org/10.1051/swsc/2024009, 2404.12164. 2

Husidic, E., N. Wijsen, I. C. Jebaraj, A. Vourlidas, L. Linan, R. Vainio, and S. Poedts, 2025. Modelling gyrosynchrotron emission from coronal energetic electrons in a CME flux rope. *Astron Astrophys*, **701**, A53. https://doi.org/10.1051/0004-6361/202555534, 2507.16449. 2

Husidic, E., N. Wijsen, L. Linan, M. Brchnelova, R. Vainio, and S. Poedts, 2024b. Cross-field Diffusion Effects on Particle Transport in a Solar Coronal Flux Rope. *ApJL*, **976**(2), L31. https://iopscience.iop.org/article/10.3847/2041-8213/ad8d56, 2411.00738. 2, 2, 9

Keppens, R., Z. Meliani, A. J. van Marle, P. Delmont, A. Vlasis, et al., 2012. Parallel, grid-adaptive approaches for relativistic hydro and magnetohydrodynamics. *J Comput Phys*, **231**, 718. https://doi.org/10.1016/j.jcp.2011.01.020. 2

Keppens, R., B. Popescu Braileanu, Y. Zhou, W. Ruan, C. Xia, Y. Guo, N. Claes, and F. Bacchini, 2023. MPI-AMRVAC 3.0: Updates to an open-source simulation framework. *Astron Astrophys*, **673**, A66. https://doi.org/10.1051/0004-6361/202245359, 2303.03026. 2

Kilpua, E. K. J., N. Lugaz, M. L. Mays, and M. Temmer, 2019. Forecasting the Structure and Orientation of Earthbound Coronal Mass Ejections. *Space Weather*, **17**(4), 498–526. https://doi.org/10.1029/2018SW001944. 2, 2

King, J., and N. Papitashvili, 2005. Solar wind spatial scales in and comparisons of hourly Wind and ACE plasma and magnetic field data. *J Geophys Res: Space Phys*, **110**(A2). https://doi.org/10.1029/2004JA010649. 2

Kirk, M., W. D. Pesnell, C. Young, and S. A. H. Webber, 2009. Automated detection of EUV Polar Coronal Holes during Solar Cycle 23. *Sol Phys*, **257**, 99–112. https://doi.org/10.1007/s11207-009-9369-y. 2

Klein, K.-L., C. S. Matamoros, and P. Zucca, 2018. Solar radio bursts as a tool for space weather forecasting. *C R Phys*, **19**(1-2), 36–42. https://doi.org/10.1016/j.crhy.2018.01.005. 2

Kliem, B., and T. Török, 2006. Torus Instability. *Phys Rev Letters*, **96**(25), 255002. https://doi.org/10.1103/PhysRevLett.96.255002, physics/0605217. 2

Koch, E., and E. W. Rosolowsky, 2015. Filament identification through mathematical morphology. *Mon Notices Royal Astron Soc*, **452**, 17. https://doi.org/10.1093/mnras/stv1521. 2

Korsós, M. B., R. Erdélyi, X. Huang, and H. Morgan, 2022. Magnetic Helicity Flux Oscillations in the Atmospheres of Flaring and Nonflaring Active Regions. *Astrophys J*, **933**(1), 66. 10.3847/1538-4357/ac7469, URL https://dx.doi.org/10.3847/1538-4357/ac7469. 2

Korsós, M. B., M. K. Georgoulis, N. Gyenge, S. K. Bisoi, S. Yu, S. Poedts, C. J. Nelson, J. Liu, Y. Yan, and R. Erdélyi, 2020. Solar Flare Prediction Using Magnetic Field Diagnostics above the Photosphere. *Astrophys J*, **896**(2), 119. https://doi.org/10.3847/1538-4357/ab8fa2. 2

Korsós, M. B., A. Ludmány, R. Erdélyi, and T. Baranyi, 2015. On flare predictability based on sunspot group evolution. *Astrophysical J letters*, **802**(2), L21. 10.1088/2041-8205/802/2/L21, URL https://dx.doi.org/10.1088/2041-8205/802/2/L21. 2

Koya, Patsourakos, S., Georgoulis, M. K, and Nindos, A., 2024. Assessment of the near-Sun magnetic field of the 10 March 2022 coronal mass ejection observed by Solar Orbiter. *Astron Astrophys*, **690**, A233. 10.1051/0004-6361/202450204, URL https://doi.org/10.1051/0004-6361/202450204. 2

Koya, S., Sarkar, R., Maharana, A., Isavnin, A., Patsourakos, S., Poedts, S., Georgoulis, M. K, Nindos, A., and Murawski, K., 2026. Constraining the magnetic flux of the CME spheromak model in EUHFORIA with the magnetic helicity budget: Case study of 10 March 2022 CME. *Astron Astrophys*, **706**, A139. 10.1051/0004-6361/202556008, URL https://doi.org/10.1051/0004-6361/202556008. 2, 2

Kumar, M., B. Kuźma, S. Poedts, K. Murawski, and E. Kilpua, 2026. Investigating the influence of the source-sink terms in a two-fluid global coronal model. *Astron Astrophys*, **707**, A21. https://doi.org/10.1051/0004-6361/202557353. 2

Kumar, M., K. Murawski, L. Kadowaki, B. Kuźma, and E. K. J. Kilpua, 2024a. Impulsively generated waves in two-fluid plasma in the solar chromosphere: Heating and generation of plasma outflows. *Astron Astrophys*, **681**, A60. https://doi.org/10.1051/0004-6361/202245638. 2

Kumar, M., K. Murawski, B. Kuźma, E. K. J. Kilpua, S. Poedts, and R. Erdélyi, 2024b. Numerical Experiment on the Influence of Granulation-induced Waves on Solar Chromosphere Heating and Plasma Outflows in a Magnetic Arcade. *Astrophys J*, **975**(1), 3. 10.3847/1538-4357/ad7464. 2

Kusano, K., Y. Bamba, T. T. Yamamoto, Y. Iida, S. Toriumi, and A. Asai, 2012. Magnetic field structures triggering solar flares and coronal mass ejections. *Astrophys J*, **760**(1), 31. Publisher: American Astronomical Society, 10.1088/0004-637x/760/1/31, URL https://iopscience.iop.org/article/10.1088/0004-637X/760/1/31. 2

Kusano, K., T. Iju, Y. Bamba, and S. Inoue, 2020. A physics-based method that can predict imminent large solar flares. *Science*, **369**(6503), 587–591. Publisher: American Association for the Advancement of Science (AAAS), 10.1126/science.aaz2511, URL https://www.science.org/doi/10.1126/science.aaz2511. 2

Kuźma, B., M. Brchnelova, B. Perri, T. Baratashvili, F. Zhang, et al., 2023. COCONUT, a Novel Fast-converging MHD Model for Solar Corona Simulations. III. Impact of the Preprocessing of the Magnetic Map on the Modeling of the Solar Cycle Activity and Comparison with Observations. *Astrophys J*, **942**, 31. 10.3847/1538-4357/aca483. 2, 2

Kuznetsov, A. A., and G. D. Fleishman, 2021. Ultimate Fast Gyrosynchrotron Codes. *Astrophys J*, **922**, 103. 10.3847/1538-4357/ac29c0. 2

Lani, A., 2009. An Object Oriented and High Performance Platform for Aerothermodynamics Simulation. Ph.D. thesis, Université Libre de Bruxelles, von Karman Institute for Fluid Dynamics, Aeronautics and Aerospace Department. URL https://difusion.ulb.ac.be/vufind/Record/ULB-DIPOT:oai:dipot.ulb.ac.be:2013/210428/Holdings. 2

Lario, D., L. Berger, L. B. Wilson III, R. B. Decker, D. K. Haggerty, E. C. Roelof, R. F. Wimmer-Schweingruber, and J. Giacalone, 2018. Flat Proton Spectra in Large Solar Energetic Particle Events. In Journal of Physics: Conference Series, vol. 1100, 012014. 10.1088/1742-6596/1100/1/012014, URL https://ui.adsabs.harvard.edu/abs/2018JPhCS1100a2014L. 2

Leitner, M., C. J. Farrugia, C. Möstl, K. W. Ogilvie, A. B. Galvin, R. Schwenn, and H. K. Biernat, 2007. Consequences of the force-free model of magnetic clouds for their heliospheric evolution. *J Geophys Res: Space Phys*, **112**(A6), A06113. 10.1029/2006JA011940. 2

Leka, K., K. Dissauer, G. Barnes, and E. L. Wagner, 2023. Properties of flare-imminent versus flare-quiet active regions from the chromosphere through the corona. II. Nonparametric discriminant analysis results from the NWRA classification infrastructure (NCI). *Astrophys J*, **942**(2), 84. DOI10.3847/1538-4357/ac9c04. 2

Linan, L., T. Baratashvili, A. Lani, B. Schmieder, M. Brchnelova, J. H. Guo, and S. Poedts, 2025. Coronal mass ejection propagation in the dynamically coupled space weather tool: COCONUT + EUHFORIA. *Astron Astrophys*, **693**, A229. https://doi.org/10.1051/0004-6361/202451854. 2

Linan, L., F. Regnault, B. Perri, M. Brchnelova, B. Kuzma, A. Lani, S. Poedts, and B. Schmieder, 2023. Self-consistent propagation of flux ropes in realistic coronal simulations. *Astron Astrophys*, **675**, A101. https://doi.org/10.1051/0004-6361/202346235. 2

Ling, L., C. Yan-mei, and L. Lei, 2020. Automatic Detection of Sunspots and Extraction of Their Feature Parameters. *Chinese Astron and Astrophys*, **44**, 462–473. https://doi.org/10.1016/j.chinastron.2020.11.003. 2

Liu, H., C. Liu, J. T. Wang, and H. Wang, 2019. Predicting solar flares using a long short-term memory network. *Astrophys J*, **877**(2), 121. DOI10.3847/1538-4357/ab1b3c. 2

Liu, J., Y. Ye, C. Shen, Y. Wang, and R. Erdélyi, 2018. A new tool for CME arrival time prediction using machine learning algorithms: CAT-PUMA. *Astrophys J*, **855**(2), 109. DOI10.3847/1538-4357/aaae69. 2

Liu, R., B. Kliem, V. S. Titov, J. Chen, Y. Wang, H. Wang, C. Liu, Y. Xu, and T. Wiegelmann, 2016. Structure, Stability, and Evolution of Magnetic Flux Ropes from the Perspective of Magnetic Twist. *Astrophys J*, **818**(2), 148. https://doi.org/10.3847/0004-637X/818/2/148. 2

Lundberg, S. M., and S.-I. Lee, 2017. A unified approach to interpreting model predictions. *Adv in neural info processing systems*, **30**. 2

Lundquist, S., 1950. Magnetohydrostatic fields. *Ark. Fys.*, **2**, 361–365. 2

Maia, D. J. F., R. Gama, C. Mercier, M. Pick, A. Kerdraon, et al., 2007. The Radio-Coronal Mass Ejection Event on 2001 April 15. *Astrophys J*, **660**, 874. 10.1086/508011. 2

Mandal, S., N. Krikova, S. Solanki, N. Sinha, and D. Banerjee, 2020. Sunspot area catalog revisited: Daily cross-calibrated areas since 1874. *Astron Astrophys*, **640**, 12. https://doi.org/10.1051/0004-6361/202037547. 2

Mann, G., A. Klassen, H. Aurass, and H. T. Classen, 2003. Formation and development of shock waves in the solar corona and the near-Sun interplanetary space. *Astron Astrophys*, **400**, 329–336. https://doi.org/10.1051/0004-6361:20021593. 2

Massa, P., and A. G. Emslie, 2022. Efficient identification of pre-flare features in SDO/AIA images through use of spatial Fourier transforms. *Frontiers Astron Space Sci*, **9**, 1040,099. https://doi.org/10.3389/fspas.2022.1040099. 2

Mikić, Z., J. A. Linker, D. D. Schnack, R. Lionello, and A. Tarditi, 1999. Magnetohydrodynamic modeling of the global solar corona. *Phys Plasmas*, **6**(5), 2217–2224. https://doi.org/10.1063/1.873474. 2

Moore, R. L., A. C. Sterling, H. S. Hudson, and J. R. Lemen, 2001. Onset of the Magnetic Explosion in Solar Flares and Coronal Mass Ejections. *Astrophys J*, **552**(2), 833–848. https://doi.org/10.1086/320559. 2

Morosan, D. E., E. K. J. Kilpua, E. P. Carley, and C. Monstein, 2019. Variable emission mechanism of a Type IV radio burst. *Astron Astrophys*, **623**, A63. 10.1051/0004-6361/201834510, 1902.01140. 2

Mugatwala, R., S. Chierichini, G. Francisco, G. Napoletano, R. Foldes, L. Giovannelli, G. De Gasperis, E. Camporeale, R. Erdélyi, and D. Del Moro, 2024. A catalogue of observed geo-effective CME/ICME characteristics. *J Space Weather Space Clim*, **14**, 6. https://doi.org/10.1051/swsc/2024004. 2, 2

Napoletano, G., R. Forte, D. Del Moro, E. Pietropaolo, L. Giovannelli, and F. Berrilli, 2018. A probabilistic approach to the drag-based model. *J Space Weather Space Clim*, **8**, A11. https://doi.org/10.1051/swsc/2018003. 2

Niemela, A., N. Wijsen, A. Aran, L. Rodriguez, J. Magdalenic, and S. Poedts, 2024. Cannibals in PARADISE: The Effect of Merging Interplanetary Shocks on Solar Energetic Particle Events. *Astrophysical J letters*, **967**(2), L35. https://doi.org/10.3847/2041-8213/ad4c70, 2405.10615. 2

Nogueira, G. A. L., R. Erdélyi, R. Wang, and K. Petrovay, 2026. Solar active region scaling laws revisited. ArXiv:2602.13677. 2

Patsourakos, S., M. Georgoulis, A. Vourlidas, A. Nindos, T. Sarris, et al., 2016. The major geoeffective Solar Eruption of 2012 March 7: comprehensive Sun-to-Earth analysis. *Astrophys J*, **817**, 14. 10.3847/0004-637X/817/1/14. 2

Patsourakos, S., and M. K. Georgoulis, 2016. Near-Sun and 1 AU magnetic field of coronal mass ejections: a parametric study. *Astrophys J*, **595**, A121. https://doi.org/10.1051/0004-6361/201628277, 1609.00134. 2

Perri, B., B. Kuźma, M. Brchnelova, T. Baratashvili, F. Zhang, P. Leitner, A. Lani, and S. Poedts, 2023. COCONUT, a Novel Fast-converging MHD Model for Solar Corona Simulations. II. Assessing the Impact of the Input Magnetic Map on Space-weather Forecasting at Minimum of Activity. *Astrophys J*, **943**(2), 124. https://doi.org/10.3847/1538-4357/ac9799, 2210.06165. 2

Perri, B., B. Kuźma, M. Brchnelova, T. Baratashvili, F. Zhang, P. Leitner, A. Lani, and S. Poedts, 2023. COCONUT, a Novel Fast-converging MHD Model for Solar Corona Simulations. II. Assessing the Impact of the Input Magnetic Map on Space-weather Forecasting at Minimum of Activity. *Astrophys J*, **943**(2), 124. https://doi.org/1538-4357/ac9799. 2

Perri, B., B. Kuźma, M. Brchnelova, T. Baratashvili, F. Zhang, et al., 2023. COCONUT, a Novel Fast-converging MHD Model for Solar Corona Simulations. II. Assessing the Impact of the Input Magnetic Map on Space-weather Forecasting at Minimum of Activity. *Astrophys J*, **943**, 124. 10.3847/1538-4357/ac9799. 2, 2

Perri, B., P. Leitner, M. Brchnelova, T. Baratashvili, B. Kuźma, F. Zhang, A. Lani, and S. Poedts, 2022. COCONUT, a Novel Fast-converging MHD Model for Solar Corona Simulations: I. Benchmarking and Optimization of Polytropic Solutions. *Astrophys J*, **936**, 19. 10.3847/1538-4357/ac7237. 2, 2, 2

Perri, B., P. Leitner, M. Brchnelova, T. Baratashvili, B. Kuźma, F. Zhang, A. Lani, and S. Poedts, 2022. COCONUT, a novel fast-converging MHD model for solar corona simulations: I. Benchmarking and optimization of polytropic solutions. *Astrophys J*, **936**(1), 19. DOI10.3847/1538-4357/ac7237. 2

Perri, S., G. Prete, G. Zimbardo, D. Trotta, L. B. Wilson III, D. Lario, S. Servidio, F. Valentini, and J. Giacalone, 2023. Interpretation of Flat Energy Spectra Upstream of Fast Interplanetary Shocks. *Astrophys J*, **950**(1), 62. 10.3847/1538-4357/acc942, URL http://dx.doi.org/10.3847/1538-4357/acc942. 2

Pick, M., 1986. Observations of Radio Continua and Terminology. *Sol Phys*, **104**(1), 19–32. 10.1007/BF00159942. 2

Pomoell, J., E. Lumme, and E. Kilpua, 2019. Time-dependent Data-driven Modeling of Active Region Evolution Using Energy-optimized Photospheric Electric Fields. *Sol Phys*, **294**(4), 41. 10.1007/s11207-019-1430-x. 2

Pomoell, J., and S. Poedts, 2018. EUHFORIA: European heliospheric forecasting information asset. *J Space Weather Space Clim*, **8**, A35. 10.1051/swsc/2018020. 2, 2

Pucha, R., K. M. Hiremath, and R. Gurumath, 2016. Development of a Code to Analyze the Solar White-Light Images from the Kodaikanal Observatory: Detection of Sunspots, Computation of Heliographic Coordinates and Area. *J Astrophys Astr*, **37**, 20. https://doi.org/10.1007/s12036-016-9370-4. 2

Pulkkinen, T., 2007. Space Weather: Terrestrial Perspective. *Living Rev Sol Phys*, **4**(1), 1. 10.12942/lrsp-2007-1. 1

Punnala, M., S. Punnala, A. Ojala, and H. Kuusniemi, 2024. The Space Economy: Review of the Current Status and Future Prospects. Springer Nature Singapore, Singapore. ISBN 978-981-97-3430-6. 10.1007/978-981-97-3430-6, URL https://doi.org/10.1007/978-981-97-3430-6. 1.1

Ravindra, B., T. G. Priya, K. Amareswari, M. Priyal, A. A. Nazia, and D. Banerjee, 2013. Development of a Code to Analyze the Solar White-Light Images from the Kodaikanal Observatory: Detection of Sunspots, Computation of Heliographic Coordinates and Area. *Astron Astrophys*, **550**, 9. https://doi.org/10.1051/0004-6361/201220416. 2

Reames, D. V., 1999. Particle acceleration at the Sun and in the heliosphere. *Space Sci Rev*, **90**, 413–491. https://doi.org/10.1023/A:1005105831781. 2

Reames, D. V., 2023. Review and outlook of solar energetic particle measurements on multispacecraft missions. *Frontiers Astron Space Sci*, **10**, 1254266. 10.3389/fspas.2023.1254266, 2307.04182. 1.2

Reames, D. V., and C. K. Ng, 1998. Streaming-limited Intensities of Solar Energetic Particles. *Astrophys J*, **504**(2), 1002–1005. 10.1086/306124, URL https://ui.adsabs.harvard.edu/abs/1998ApJ...504.1002R. 8, 2

Richardson, I. G., and H. V. Cane, 2010. Near-Earth interplanetary coronal mass ejections during solar cycle 23 (1996–2009): Catalog and summary of properties. *Sol Phys*, **264**, 189–237. https://doi.org/10.1007/s11207-010-9568-6. 2

Riley, P., M. L. Mays, J. Andries, T. Amerstorfer, D. Biesecker, et al., 2018. Forecasting the arrival time of coronal mass ejections: Analysis of the CCMC CME scoreboard. *Space weather*, **16**(9), 1245–1260. https://doi.org/10.1029/2018SW001962. 2

Rosner, R., W. H. Tucker, and G. Vaiana, 1978. Dynamics of the quiescent solar corona. *Astrophys J*, **220**, 643–645. 2

Salman, T. M., T. Nieves-Chinchilla, L. K. Jian, N. Lugaz, F. Carcaboso, E. E. Davies, and Y. M. Collado-Vega, 2024. A Survey of Coronal Mass Ejections Measured In Situ by Parker Solar Probe during 2018–2022. *Astrophys J*, **966**(1), 118. 10.3847/1538-4357/ad320c, URL https://dx.doi.org/10.3847/1538-4357/ad320c. 2

Salman, T. M., R. M. Winslow, and N. Lugaz, 2020. Radial Evolution of Coronal Mass Ejections Between MESSENGER, Venus Express, STEREO, and L1: Catalog and Analysis. *J Geophys Res: Space Phys*, **125**(1), e27084. https://doi.org/10.1029/2019JA027084, 1912.11731. 2

Sammis, I., F. Tang, and H. Zirin, 2000. The Dependence of Large Flare Occurrence on the Magnetic Structure of Sunspots. *Astrophys J*, **540**(1), 583. 10.1086/309303, URL https://dx.doi.org/10.1086/309303. 2

Scholl, I., and S. R. Habbal, 2008. Automatic Detection and Classification of Coronal Holes and Filaments Based on EUV and Magnetogram Observations of the Solar Disk. *Sol Phys*, **248**, 425–429. https://doi.org/10.1007/s11207-007-9075-6. 2

Schrijver, C. J., 2007. A Characteristic Magnetic Field Pattern Associated with All Major Solar Flares and Its Use in Flare Forecasting. *Astrophysical J letters*, **655**(2), L117–L120. 10.1086/511857. 2, 2

Schrijver, C. J., K. Kauristie, A. D. Aylward, C. M. Denardini, S. E. Gibson, et al., 2015. Understanding space weather to shield society: A global road map for 2015-2025 commissioned by COSPAR and ILWS. *Adv Space Res*, **55**(12), 2745–2807. https://doi.org/10.1016/j.asr.2015.03.023, 1503.06135. 1

Schwenn, R., 2006. Space Weather: The Solar Perspective. *Living Rev Sol Phys*, **3**(1), 2. https://doi.org/10.12942/lrsp-2006-2. 2

Selvaraju, R. R., M. Cogswell, A. Das, R. Vedantam, D. Parikh, and D. Batra, 2017. Grad-cam: Visual explanations from deep networks via gradient-based localization. In Proceedings of the IEEE international conference on computer vision, 618–626. 2

Shibata, K., and T. Magara, 2011. Solar Flares: Magnetohydrodynamic Processes. *Living Rev Sol Phys*, **8**(1), 6. https://doi.org/10.12942/lrsp-2011-6. 2

Shih, F., and A. Kowalski, 2003. Automatic Extraction of Filaments in Hα Solar Images. *Sol Phys*, **218**, 99–122. https://doi.org/10.1023/B:SOLA.0000013052.34180.58. 2

Stenning, D., T. Lee, D. van Dyk, V. Kashyap, J. Sandell, and C. Young, 2013. Morphological feature extraction for statistical learning with applications to solar image data. *Statis Analy Data Mining*, **6**, 329–345. https://doi.org/10.1002/sam.11200. 2

Stepanyuk, O., K. Kozarev, and M. Nedal, 2022. Multi-scale image preprocessing and feature tracking for remote CME characterization. *J Space Weather Space Clim*, **12**, 20. https://doi.org/10.1051/swsc/2022020. 2

Sun, D., X. Huang, Z. Zhao, and L. Xu, 2023. Deep Learning–based Solar Flare Forecasting Model. III. Extracting Precursors from EUV Images. *Astrophys J Supplements*, **266**(1), 8. DOI10.3847/1538-4365/acc248. 2

Talafha, M., M. Nagy, A. Lemerle, and K. Petrovay, 2022. Role of observable nonlinearities in solar cycle modulation. *Astrophys J*, **660**, A92. https://doi.org/10.1051/0004-6361/202142572. 2

Temmer, M., 2021. Space weather: the solar perspective: An update to Schwenn (2006). *Living Rev Sol Phys*, **18**(1), 4. https://doi.org/10.1007/s41116-021-00030-3, 2104.04261. 1

Thernisien, A., R. Howard, and A. Vourlidas, 2008. Modeling of Flux Rope Coronal Mass Ejections. *Astrophys J*, **652**, 763. 10.1086/508254. 2

Thernisien, A., A. Vourlidas, and R. A. Howard, 2009. Forward Modeling of Coronal Mass Ejections Using STEREO/SECCHI Data. *Sol Phys*, **256**(1-2), 111–130. 10.1007/s11207-009-9346-5. 2

Titov, V. S., and P. Démoulin, 1999. Basic topology of twisted magnetic configurations in solar flares. *Astron Astrophys*, **351**, 707–720. 2

Titov, V. S., T. Török, Z. Mikic, and J. A. Linker, 2014. A Method for Embedding Circular Force-free Flux Ropes in Potential Magnetic Fields. *Astrophys J*, **790**(2), 163. https://doi.org/10.1088/0004-637X/790/2/163. 2

Török, T., B. Kliem, and V. S. Titov, 2004. Ideal kink instability of a magnetic loop equilibrium. *Astron Astrophys*, **413**, L27–L30. https://doi.org/10.1051/0004-6361:20031691, astro-ph/0311198. 2

Tun, S. D., and A. Vourlidas, 2013. Derivation of the Magnetic Field in a Coronal Mass Ejection Core via Multi-frequency Radio Imaging. *Astrophys J*, **766**, 130. 10.1088/0004-637X/766/2/130. 2

van den Berg, J., D. T. Strauss, and F. Effenberger, 2020. A Primer on Focused Solar Energetic Particle Transport. *Space Sci Rev*, **216**(8), 146. 10.1007/s11214-020-00771-x. 2

Verbeke, Pomoell, J., and Poedts, S., 2019. The evolution of coronal mass ejections in the inner heliosphere: Implementing the spheromak model with EUHFORIA. *Astron Astrophys*, **627**, A111. https://doi.org/10.1051/0004-6361/201834702. 2

Verbeke, C., T. Baratashvili, and S. Poedts, 2022. ICARUS, a new inner heliospheric model with a flexible grid. *Astron Astrophys*, **662**, A50. https://doi.org/10.1051/0004-6361/202141981. 2

Volpes, L., and V. Bothmer, 2015. An application of the stereoscopic self-similar-expansion model to the determination of CME-driven shock parameters. *Sol Phys*, **290**, 3005–3022. https://doi.org/10.1007/s11207-015-0775-z. 2

Vourlidas, A., S. Patsourakos, and N. Savani, 2019a. Predicting the geoeffective properties of coronal mass ejections: current status, open issues and path forward. *Philosophical Transactions of the Royal Society A*, **377**(2148), 20180,096. http://doi.org/10.1098/rsta.2018.0096. 2

Vourlidas, A., S. Patsourakos, and N. P. Savani, 2019b. Predicting the geoeffective properties of coronal mass ejections: current status, open issues and path forward. *Philosophical Transactions of the Royal Society A: Mathematical, Physical and Engineering Sciences*, **377**(2148), 20180,096. 10.1098/rsta.2018.0096, URL https://doi.org/10.1098/rsta.2018.0096. 2

Vršnak, B., T. Žic, D. Vrbanec, M. Temmer, T. Rollett, et al., 2013. Propagation of interplanetary coronal mass ejections: The drag-based model. *Sol Phys*, **285**, 295–315. https://doi.org/10.1007/s11207-012-0035-4. 2

Wagner, A., S. Bourgeois, E. K. J. Kilpua, R. Sarkar, D. J. Price, et al., 2024a. The automatic identification and tracking of coronal flux ropes. II. New mathematical morphology-based flux rope extraction method and deflection analysis. *Astron Astrophys*, **683**, A39. http://dx.doi.org/10.1051/0004-6361/202348113. 2, 2, 2

Wagner, A., E. K. J. Kilpua, R. Sarkar, D. J. Price, A. Kumari, F. Daei, J. Pomoell, and S. Poedts, 2023. The automatic identification and tracking of coronal flux ropes. I. Footpoints and fluxes. *Astron Astrophys*, **677**, A81. https://doi.org/10.1051/0004-6361/202346260. 2, 2

Wagner, A., D. J. Price, S. Bourgeois, F. Daei, J. Pomoell, S. Poedts, A. Kumari, T. Barata, R. Erdélyi, and E. K. J. Kilpua, 2024b. The effect of data-driving and relaxation models on magnetic flux rope evolution and stability. *Astron Astrophys*, **692**, A74. https://doi.org/10.1051/0004-6361/202450577. 2

Wagner, A., D. J. Price, S. Bourgeois, J. Pomoell, S. Poedts, and E. K. J. Kilpua, 2024c. Solar magnetic flux rope identification with GUITAR: GUI for Tracking and Analysing flux Ropes. *Frontiers Astron Space Sci*, **11**, 1383072. https://doi.org/10.3389/fspas.2024.1383072. 2, 2

Wang, C., D. Du, and J. D. Richardson, 2005. Characteristics of the interplanetary coronal mass ejections in the heliosphere between 0.3 and 5.4 AU. *J Geophys Res: Space Phys*, **110**(A10). https://doi.org/10.1029/2005JA011198, https://agupubs.onlinelibrary.wiley.com/doi/pdf/10.1029/2005JA011198. 2

Wang, H., Y. Cui, R. Li, L. Zhang, and H. Han, 2008. Solar flare forecasting model supported with artificial neural network techniques. *Adv Space Res*, **42**(9), 1464–1468. https://doi.org/10.1016/j.asr.2007.06.070. 2

Wang, Y., B. Wang, C. Shen, F. Shen, and N. Lugaz, 2014. Deflected propagation of a coronal mass ejection from the corona to interplanetary space. *J Geophys Res: Space Phys*, **119**(7), 5117–5132. https://doi.org/10.1002/2013JA019537, 1406.4684. 2

Webb, D. F., and T. A. Howard, 2012. Coronal Mass Ejections: Observations. *Living Rev Sol Phys*, **9**(1), 3. 10.12942/lrsp-2012-3. 1.2

Welsch, B. T., Y. Li, P. W. Schuck, and G. H. Fisher, 2009. What is the relationship etween photospheric flow Fields and solar flares? *Astrophys J*, **705**(1), 821–843. https://doi.org/10.1088/0004-637X/705/1/821. 2

Wijsen, N., 2020. PARADISE: A model for energetic particle transport in the solar wind. PhD dissertation, KU Leuven (Belgium) and Univ. Barcelona (Spain). 2

Wijsen, N., A. Aran, J. Pomoell, and S. Poedts, 2019. Spreading protons in the heliosphere: a note on cross-field diffusion effects. In Journal of Physics Conference Series, vol. 1332 of *J. Phys. Conf. Ser.*, 012018. IOP. https://doi.org/10.1088/1742-6596/1332/1/012018, 1908.00769. 2

Winslow, R. M., N. Lugaz, L. C. Philpott, N. A. Schwadron, C. J. Farrugia, B. J. Anderson, and C. W. Smith, 2015. Interplanetary coronal mass ejections from MESSENGER orbital observations at Mercury. *J Geophys Res: Space Phys*, **120**(8), 6101–6118. https://doi.org/10.1002/2015JA021200, https://agupubs.onlinelibrary.wiley.com/doi/pdf/10.1002/2015JA021200, URL https://agupubs.onlinelibrary.wiley.com/doi/abs/10.1002/2015JA021200. 2

Wójcik, D., B. Kuźma, K. Murawski, and A. K. Srivastava, 2019. Two-fluid Numerical Simulations of the Origin of the Fast Solar Wind. *Astrophys J*, **884**(2), 127. https://doi.org/10.3847/1538-4357/ab26b1, 1906.01897. 2

Xia, C., J. Teunissen, I. El Mallah, E. Chané', and R. Keppens, 2018. MPI-AMRVAC 2.0 for Solar and Astrophysical Applications. *Astrophys J*, **234**, 30. https://doi.org/10.3847/1538-4365/aaa6c8. 2

Yashiro, S., N. Gopalswamy, G. Michalek, O. St. Cyr, S. Plunkett, N. Rich, and R. Howard, 2004. A catalog of white light coronal mass ejections observed by the SOHO spacecraft. *J Geophys Res: Space Phys*, **109**(A7). https://doi.org/10.1029/2003JA010282. 2

Zhao, C., G. Lin, Y. Deng, and X. Yang, 2016. Automatic Recognition of Sunspots in HSOS Full–Disk Solar Images. *P Astron Soc Australia*, **33**, 9. https://doi.org/10.1017/pasa.2016.17. 2

Žic, T., B. Vršnak, and M. Temmer, 2015. Heliospheric propagation of coronal mass ejections: Drag-based model fitting. *Astrophys J Supplements*, **218**(2), 32. https://doi.org/10.1088/0067-0049/218/2/32. 2